MT-CWJCR-095-029

ANNUAL REPORT

Pressureless Infiltration of Ceramics by Molten Metals

Submitted to:

Dr. Steven G. Fishman
Office of Naval Research
800 North Quincy Street
Arlington, VA 22217

Submitted by:

P.R. Chidambaram and G.R. Edwards
Center for Welding, Joining, and Coatings Research
Colorado School of Mines
Golden, CO 80401

Research Performed Under Contract N00014-95-1-0066

December, 1995

CSM

CENTER FOR WELDING AND JOINING RESEARCH

Colorado School of Mines
Golden, Colorado 80401

DEPARTMENT OF THE NAVY
OFFICE OF NAVAL RESEARCH
SEATTLE REGIONAL OFFICE
1107 NE 45TH STREET, SUITE 350
SEATTLE WA 98105-4631

IN REPLY REFER TO:

4330
ONR 247
11 Jul 97

From: Director, Office of Naval Research, Seattle Regional Office, 1107 NE 45th St., Suite 350, Seattle, WA 98105
To: Defense Technical Center, Attn: P. Mawby, 8725 John J. Kingman Rd., Suite 0944, Ft. Belvoir, VA 22060-6218

Subj: RETURNED GRANTEE/CONTRACTOR TECHNICAL REPORTS

1. This confirms our conversations of 27 Feb 97 and 11 Jul 97. Enclosed are a number of technical reports which were returned to our agency for lack of clear distribution availability statement. This confirms that all reports are unclassified and are "APPROVED FOR PUBLIC RELEASE" with no restrictions.

2. Please contact me if you require additional information. My e-mail is *silverr@onr.navy.mil* and my phone is (206) 625-3196.

ROBERT J. SILVERMAN

Project Summary

Pressureless infiltration of molten metals into ceramics is perhaps the most cost-effective approach to liquid-metal processing of metal-matrix composites. Two approaches are currently being investigated for their respective pressureless infiltration potential.

A "carrier oxide" approach to infiltration relies on the use of a intermediary liquid oxide which carriers the liquid metal into the capillary channels of the porous ceramic. The effectiveness of this approach was discovered by understanding the nature of wetting and spreading in copper-oxygen and copper-titanium alloy liquids in contact with alumina substrates

Aluminum oxide, a relatively cheap reinforcing material, does not develop an interface with liquid aluminum, but titanium readily wets aluminum oxide. Titanium-coated aluminum oxide surfaces are energetically conducive to the pressureless infiltration of liquid aluminum.

Results from the above two approaches are discussed in detail in the following sections.

Plans for Next Year Research

The property requirements of the carrier oxide include the ability to wet the ceramic and the liquid metal simultaneously. Various oxide systems are currently being investigated for their potential as carrier oxides. Experiments to evaluate the interfacial

energy between the liquid metal and the liquid oxide are being investigated. The carrier oxide principle was conceived based on the results from the experiments on copper/copper-oxide; high volume fractions of copper- oxide disperssed within the mettalic matrix can embrittle the composites. Possible applications in this system suffer from the large oxygen concentration in the resulting composite. An infiltration process wherein the oxide is formed insitu within the melt could reduce the final oxygen concentration, and improve the mechanical integrity of the composite. Detailed phase equilibria calculations are underway to investigate the gas phase oxidation feasibility.

Project Accomplishments

Papers Published in Refereed Journals

- Chidambaram, A. Meier, and G.R. Edwards, "The Nature of Interfacial Phenomena at Copper-Titanium/Alumina and Copper-Oxygen/Alumina Interfaces", accepted for publication in the Materials Science and Engineering.
- Meier, P.R. Chidambaram, and G.R. Edwards, "A Comparison of the Wettability of Copper-Copper Oxide and Silver-Copper Oxide on Polycrystalline Alumina", accepted for publication in the Journal of Materials Science.

Presentations

- P.R. Chidambaram, A. Meier, G.R. Edwards, and L. Koland, "A Novel Approach to Join Ceramics to Metals: Aggressively Wetting Systems", presented at the 76th American Welding Society Annual Convention, Cleveland, Ohio (April 1995).

Wetting In Copper-Oxygen And Copper-Titanium Systems And Pressureless-Infiltration By Intermediate Liquid Oxides

Introduction

Traditionally, the contact angle and the associated analysis based on the Young equation has been used extensively to describe the complex phenomena occurring at the liquid metal-ceramic interface [1-2]. The analysis presented in the literature is based on the sessile drop experiment. The general case of a liquid metal in contact with the ceramic is shown in Figure 1, where a balance of surface tension forces results in the familiar Young equation:

$$\gamma^{lv} \mathrm{Cos}\theta = \gamma^{sv} - \gamma^{sl} \qquad 1$$

In this expression, γ^{sv}, γ^{lv} and γ^{sl} are the corresponding surface energies of solid/vapor, liquid/vapor and solid/liquid interfaces, respectively. The wettability parameter, $\gamma^{lv} \cos\theta$, describes the wetting tendency of the liquid on the solid substrate.

Based on the nature of the attractive forces, wetting can be classified as physical or chemical. Physical wetting can be defined as the phenomenon observed in a solid-liquid system where the interface formation is energetically favored by the reversible physical forces across the interface. Van der Waals forces and electrostatic attractions are examples of such physical forces. In these situations, the Young equation can be applied without ambiguity.

Interface formation by virtue of chemical bonds across the interface can be defined as chemical wetting. Chemical bonds are formed when the electronic structure of the surface atoms of both the mating species are altered. Such changes occur by a charge transfer reaction (redox) or by a simple mixing process of one phase dissolving within the other. These two different chemical wetting mechanisms are referred to as redox wetting and solution wetting respectively.

In chemically wetting systems, there are no ambiguities when the drop assumes an obtuse angle and the system is considered non-wetting. However, when the drop assumes an acute angle, a reaction product always forms at the liquid metal/ceramic interface [3,4]. Formation of a reaction product naturally interposes a new interface. The classic Young equation is inadequate to describe the interface where a new reaction layer is formed.

When a metallic liquids contacts a ceramic substrate, the liquid metal wets the reaction product rather than the ceramic surface, and the measured contact angle is determined by the reaction product and not by the ceramic itself. These two facts were proved, based on elegant experimentation on reactive wetting systems, by Eustathopolous and co-workers [5,6]. Espie et al. [5] showed that the measured contact angles were nearly equal when liquid copper-palladium-titanium alloy was in contact with three different oxide ceramics such as alumina, mullite and silicon dioxide. Upon characterizing

the interface, they found that in all three cases the reaction product was titanium trioxide. In another similar study, Kritsalis et al. [6] tracked the change in contact angle as a function of the titanium concentration for liquid nickel- palladium-titanium alloys in contact with alumina. Three contact angle plateaus, corresponding to three different reaction products, were observed. It is evident that at the reactive metal/ceramic interface, the observed acute angle is a consequence of reaction layer formation at the interface.

As mentioned earlier, chemical wetting occurs as a result of two very different reactions - redox and solution reactions. Copper-titanium alloys in contact with alumina reduce the ceramic surface to develop a reaction product, while liquid copper-oxygen alloys in contact with alumina mutually dissolve to form a spinel reaction product. Both alloys exhibit an acute contact angle in contact with polycrystalline alumina [1,7,8,9].

In solution wetting (copper-oxygen alloys) systems, in contrast to the redox wetting (copper-titanium alloys) systems, the equilibrium contact angle develops rather rapidly and does not change as a function of time. Also, these liquids have been observed to infiltrate microcapillary channels in alumina [10].

The dynamics of a liquid alloy drop spreading on a ceramic can be studied as two distinct phenomena, as shown in Figure 2. In Stage I, a reaction layer forms beneath the liquid drop, and in Stage II, the liquid drop spreads beyond the original triple point. When the reactive alloy first comes in contact with the ceramic substrate, no reaction has occurred; hence, the drop does not yet wet the ceramic surface. In this situation, the

interfacial energy, γ^{sl}, is large and can be calculated using the Young equation. The alloy then reacts with the ceramic, and the formation of the reaction product causes both the interfacial energy to decrease and the liquid drop to assume an acute angle. This decrease in contact angle has been verified to be a function of time [1]. Naidich [1] and Aksay et. al [11] have modeled the contact angle and spreading in reactive wetting in terms of the free energy of reaction at the interface. And calculated an interfacial energy term based on the decrease in the free energy by reaction. However, this approach has been disputed recently [5]. Furthermore, there are no experiments published in the literature that provide indisputable evidence as to the importance of the free energy term. Therefore, the driving force for the movement of the liquid onto unreacted surface to form an acute angle is not clearly understood. There are three possibilities: a) the solid surface develops a long range attractive force that pulls the liquid to unreacted areas; b) the lowering of the interfacial energy under the drop pushes the drop ahead of the original triple point; or c) the hydrostatic head of the liquid drop causes the drop to spread under the influence of external driving forces such as gravity. The actual driving force could be a combination of these forces.

This research is an attempt both to document the difference and try to understand the differences in the wetting behavior of copper-oxygen alloy liquids (solution wetting) and purely metallic liquids such as copper-titanium (redox wetting) alloys on alumina

surfaces. Both systems were tested for wettability and the ability to infiltrate in the traditional sessile drop and capillary rise configurations.

Experimental Procedure

The wetting, spreading and infiltration behavior of both the systems was characterized by three different experiments. In the first phase, classical sessile drop measurements were made using a tube furnace with a viewing window (Figure 3). This system recirculated argon through an oxygen scavenger to reduce the oxygen concentration to 0.006 Pa. The substrate was Coors AD-996 electronic grade alumina (99.6% purity, 3 micron surface finish) and copper (99.99% purity), titanium (99.99% purity) and copper oxide (CuO) powder (99.9% purity). The alumina samples were cleaned with nitric acid and rinsed with ethanol before testing. Copper containing 6 and 8.5 w/o-titanium or 3-w/o oxygen were used in this study. Each Cu-Ti alloy sample was alloyed during the test, a drop of molten copper was dropped onto a thin plate of titanium at 1120°C to obtain true isothermal spreading data. The detailed experimental approach to accomplish the isothermal spreading of copper-titanium alloys on alumina surfaces is discussed elsewhere [8]. The total metal weight was 1.200 ± 0.005 grams. Copper oxide powder was boxed in a copper foil to form the copper-copper oxide liquid mixture [9]. These tests were also conducted at an argon overpressure of approximately 10 kPa, while

the temperature was maintained at 1300°C. Since copper oxide was introduced in the form of a powder, true isothermal spreading could not be measured. The spreading of the drops was videotaped, and the spread diameter was measured as a function of time by analyzing frames of the videotape on a Leco image analyzer. These measurements were accurate to within ± 0.1 mm.

In the second phase of experimentation, the ability of the liquid mixtures to penetrate the pores in alumina was investigated. A 35-volume-percent-porosity alumina filter tube with a 4 mm capillary was placed on the copper-based alloy mixtures described above and melted in the furnace system previously described at 1300°C. The samples were cooled and examined for infiltration of the liquid into the porous ceramic.

A better controlled experimental apparatus using the capillary rise principle was used to test the ability of the copper-titanium liquids to infiltrate the capillary tube in the third phase of experimentation. The details of the experimental procedures are discussed elsewhere [4]; a schematic diagram of the apparatus is reproduced in Figure 4. Coors AD-998 4-mm diameter tubes were immersed into copper-6 and 8.5-w/o titanium liquid at 1150°C for 3600 seconds. More than 100 grams of titanium pellets placed next to the crucible containing the molten alloy maintained the oxygen partial pressure below pressure required to oxidize the titanium in the alloy.

Results & Discussions

In the sessile drop configuration, both the copper-titanium alloy and the copper-oxygen alloy spread to assume an acute contact angle; however, the spreading behavior was very different. The copper-titanium alloy spread at a measurable rate. The diameter and contact angles of the drops, measured as a function of time, is plotted in Figure 5 a and 5 b respectively. The spreading rates reported here are relatively slower than the rates reported by Kritsalis et. al [2]. We believe that the apparently slower rate stems from the differences in the experimental techniques used. The experiments conducted here are based on true isothermal study where the time zero corresponds to the exact instance when the liquid contacts the ceramic surface. The data reported in the literature [2] includes studies where the alloy was placed as a solid on the ceramic substrate and heated up to the test temperature. This approach results in significant spreading before the destination temperature is reached. Also, the test sample configurations and atmosphere play a critical role, this is the subject of the paper due to be published in Journal of Materials Science [8].

The copper-oxygen alloy rapidly reached a equilibrium configuration and the drop diameter did not increase with increasing hold times. In fact, the drop started to spread even before the destination temperature, 1300°C, was reached. This behavior is not

surprising since the eutectic temperature in the copper-oxygen phase diagram in the copper-rich region is only 1060°C. Spreading can occur the moment the eutectic melt is formed. After extended holding times at temperature, the copper-oxygen alloy drops receded from the widest spreading diameters. The oxygen from the drop was lost to the atmosphere, and an apparent decrease in the oxygen activity in the liquid drop caused the drops to recede [9]. The measured drop diameter was used to calculate an apparent contact angle using established procedures [12]. The drops were assumed to be truncated spheres, and the density of the drop was assumed to be the density of pure copper for the copper-oxygen alloys and was calculated based on a rule of mixtures approximation for the copper-titanium alloys. The equilibrium contact angles calculated from the measured drop diameters are shown in Table 1.

In the second phase of experimentation, the two liquids demonstrated interestingly different infiltration characteristics. The copper-oxygen alloy infiltrated the porous ceramic and formed a homogeneous composite; however, the copper-titanium alloy did not infiltrate the micro-capillary channels in the porous alumina. The apparently anomalous behavior of the copper-titanium liquid could result from one of the following three reasons: a) the driving force for reactive metal liquid to move to unreacted ceramic surface is inherently low, b) the titanium oxide layer formation prevented the liquid alloy from

infiltrating the small pores in alumina or c) the reaction layer formation kinetics are very slow.

The macrograph in Figure 6 is a cross-section of the porous alumina tube with the capillary section in the middle. As can be seen in the figure, the copper 3-w/o oxygen alloy infiltrated the pores and rose in the capillary tube. The liquid morphology in cross-section is also shown as a schematic in Figure 6 b and c. The reaction layer that forms has been identified to be a spinel phase [9]. The solidified liquid morphology reveals some interesting aspects of the infiltration behavior. Two different phases can be clearly delineated in the micrograph. These two phases correspond to the L_1 & L_2 liquids that were immiscible at the operating temperature. The copper-oxygen phase diagram in Figure 7a shows the miscibility gap [13]. According to this diagram, at 1300°C the nominal composition of the alloy does not fall in the two-phase region; however, considerable discrepancies concerning the location of the miscibility gap appear in the copper-oxygen diagrams published in the literature. Such discrepancies are illustrated in Figure 7b [14]. The most recent phase diagram is shown in Figure 7a. Also, when copper-oxygen liquid is in contact with alumina, some alumina dissolves in the liquid, thereby increasing the oxygen content in the liquid. Therefore, it is reasonable to expect the two liquid phases to separate at the experimental temperature. Also, the phase separation as seen in Figure 6

could not have occurred during rather rapid cooling, where the liquid solidifies relatively rapidly.

The oxygen rich, less dense, and darker L_2 liquid develops a wetting meniscus, while the copper-rich L_1 liquid develops a non-wetting, convex meniscus. At the infiltration temperature, the L_2 liquid wets the alumina surface, aggressively progresses to unreacted surfaces, and in the process, carries the L_1 liquid through the pores of the alumina. It is energetically unfavorable to leave the L_1 liquid behind because two new surfaces would have to be created at the L_1/L_2 interface.

The third phase of experimentation, using the capillary rise apparatus, was specifically designed to understand why the copper-titanium liquid does not infiltrate. The titanium sponge, placed next to the crucible, maintained the oxygen partial pressure at the pure titanium/titanium oxide equilibrium. The oxygen partial pressure required to oxidize the titanium in the copper alloy containing either 6 or 8.5-w/o titanium is certainly more than the pure titanium/titanium oxide equilibrium pressure. Nonetheless, liquid copper-titanium alloy did not rise within the capillary tube during this test. Upon solidification and further cooling to room temperature, reacted and unreacted areas of the alumina tube could be delineated very clearly. Close inspection revealed that the liquid level inside the tube was lower than the level outside. The macrograph in Figure 8 a shows the cross-section of the capillary tube immersed in copper-6- w/o titanium alloy for 3600 seconds. The schematic diagrams in Figure 8 b and c summarize the observations. Figure 8b

corresponds to a situation where the alumina tube is just immersed in the molten metal, while Figure 8c illustrates the morphology upon withdrawing the tube from the melt after a 3600-s immersion. The reaction layer forms on the surface of the tube in contact with the liquid. Even immersions up to 3600 s do not result in any capillary rise. When the ceramic tube was pulled out of the liquid, the liquid height remained at the original level. In other words, once the reaction layer formed, raising the tube above the melt surface, caused the liquid metal to be maintained at the original level. When the tube was immersed to a greater depth into the molten copper-titanium alloy, the reaction layer formed on the larger fraction of the inside surface of the alumina tube that was now exposed to the melt. Upon withdrawing the tube from this immersion depth, the liquid that remained in the capillary tube was entirely in contact with the reaction layer on the inside surface of the tube. And in this situation, the liquid developed a concave, wetting meniscus. The cross-section of the alumina tube shown in Figure 9 a and the schematic figure in 9 b and c correspond to this situation.

The images recorded from both liquids using the video camera in the sessile drop experiment were studied for any observable differences in the drop morphology during the spreading process. The sets of sessile drops in Figure 10 were recorded at various times for the copper-3-w/o oxygen alloy spreading on alumina. The schematic figures are drawn to better illustrate the drop morphologies. The drop melted even before the test temperature was reached and the drop attained the stationary contact angle rather rapidly,

therefore the times are not marked in Figure 10. The similar pictures and schematic diagram for the copper-titanium alloy are shown in Figure 11. The times when the images were recorded are shown in Figure 11. It can be clearly seen from these two figures that the drop morphologies during the various stages of spreading of these two alloys are very different. The copper-oxygen alloy assumes drop shapes typical of liquids which encounter a classic wetting situation. However, the copper-titanium liquid develops a "mushroom-shaped" droplet before the liquid actually spreads further. This behavior can be expected when gravity aids the spreading of the copper-titanium liquid or when the liquid vapor surface tension decreases with time. In the present experiment on copper-titanium alloys, it is hard to determine which of the two phenomena is dominant. In contrast, the copper oxygen liquid drop morphologies (shown in the schematic diagram) develop rapidly. The final drop shape is attained within a few minutes after melting.

Based on the observations presented here, it is clear that the wetting and infiltration behavior of the two liquids are very different. The differences stem from the fact that the inherent driving force for the copper-titanium liquid alloy to contact unreacted areas is very low. It has been established that the rate reaction layer formation in the copper-titanium/alumina system is relatively slower than similar reaction rates in the copper-oxygen alloy/alumina system [7,15]. In the sessile drop configuration, gravity aids in the spreading of reactive metals, while the gravity force works against the liquid in the capillary rise configuration. Other driving forces, such as the decrease in the interfacial

energy beneath the liquid drop, and the decrease in the liquid vapor surface energy, also contribute to the differences. It is difficult experimentally to determine the relative contributions from the various forces.

The copper-oxygen alloys (in the presence of oxygen rich L_2 liquid) possess a driving force when spreading on alumina which is sufficiently large to force the liquid into contact with fresh areas of the ceramic. Hence the spreading and infiltration of these liquids is much more aggressive than that for the redox wetting liquid. This type of affinity of the oxygen-rich liquid to cover unreacted areas is certainly related to the force of attraction between the ions on the ceramic surface and the ions in the liquid. When the liquid metal contains significant moles of oxygen, the liquid can be considered partially ionic and the anions and the cations in the liquid form a dipole. The dipoles present in the liquid are attracted to similar dipoles in the solid ceramic surface with an attractive force similar to a van der Waals type dispersion force. Quantitative estimations of these forces are beyond the scope of this paper because suitable calculation must include summation over all the lattice sites and integration of frequency-dependent, complex dielectric constants.

Physical attraction forces of the van der Waals type have been termed long range forces because, these forces decay as a function of distance squared for situations where two blocks of material are systematically separated. Perhaps such long range forces provide the energy required for the copper-oxygen alloy to spread to unreacted areas of

the ceramic. The magnitudes of these forces must be very small, of the order of a few hundred mJ/m^2. The equilibrium interfacial energy required to develop a contact angle of 15 degrees in the copper-titanium alumina system is of the order of 1500 mJ/m^2. Consequently, it is obvious that the van der Waals forces are not fully responsible for the resultant wetting. Formation of a reaction product, (copper-aluminum oxide spinel in the case of copper-copper oxide liquid in contact with alumina) and the associated decrease in the interfacial energy allows the contact angles to reach such low numbers.

In purely metallic liquids, although a reaction layer forms, no long range attractive forces develop. When a reaction layer forms the electronic structure changes occur on an atomic scale, and these highly localized forces are not sufficient to draw the liquid to unreacted areas.

Based on the various stages discussed in the introduction for the spreading of a liquid in a sessile drop configuration (Figure 2), the following mechanism can be proposed for the spreading of either liquid: the instance both the copper-titanium and copper-oxygen liquids contact alumina, no reaction layer is present and the interfacial energy here corresponds to a non-wetting situation. At this point, the liquid reacts with the substrate. The kinetics of dissolution at the copper-oxygen alloy/alumina interface are much faster than the reduction reaction at the copper-titanium/alumina interface [7,15]. Also, the weak long range forces developed by the copper-oxygen alloy (particularly L_2) draw the liquid to unreacted areas, and the final equilibrium contact angle develops rather rapidly. In the

case of the copper-titanium alloy, the reaction layer forms by a nucleation and growth process, and the formation of the reaction product causes a decrease in the interfacial energy. This low reaction layer formation kinetics, coupled with the hydrostatic head of the liquid drop, causes the liquid to move ahead of the original triple point at a slow rate.

Liquid metal/ceramic interfaces play an important role both in the processing of metal matrix composites and in the brazing of metals to ceramics. The above discussion and the two apparently different spreading behaviors impact both these technologies. A liquid that exhibits an inherent driving force to move to unreacted areas of the ceramic implies that metal-matrix composites using this route can be manufactured by a pressureless process. A pressureless infiltration process is a significantly more cost-effective manufacturing process for composites compared to the currently used squeeze-casting process.

The metal matrix composites currently in use, such as aluminum/silicon carbide, rely primarily on the reduction reaction for interface formation. As shown in this paper, these liquids only react with the ceramic on contact and do not exhibit an inherent driving force to move to unreacted areas. Successful processing approaches for the manufacture of these composites that rely on redox reactions have always used some mechanical means to move the liquid to unreacted areas.

Similar issues apply to joining technology. The copper-oxygen alloy liquids wet, spread and fill in the micro-capillary channels present on the ceramic, as opposed to

copper-titanium brazing liquids that only react on contact. Direct bonding or eutectic joining is a commercial joining technique in which the copper is oxidized to copper oxide on the faying surface and brazed to the ceramic. Presence of oxygen at the interface does deteriorate the mechanical properties of the interface, and it is the future challenge of material scientists to take advantage of the oxygen during processing, but distribute the oxygen away from the interface to improve the mechanical properties.

Although our findings are from the copper-titanium and copper-oxygen systems alone, we believe that our results and the associated discussions are equally valid for other reduction reaction-based reactive metal and solution wetting systems in contact with alumina as well, since systems in each of these two groups exhibit similar wetting behavior on alumina surfaces.

Conclusions

Copper-titanium alloy liquids in contact with alumina form a reaction layer by a reduction reaction. The kinetics of sessile drop spreading is relatively slow. These liquids develop localized short range attractive forces with alumina that require an external force to move the liquid to unreacted areas. On the contrary, copper-oxygen alloys which react by a dissolution reaction, aggressively spread on alumina surfaces and develop equilibrium angles rapidly. Copper-oxygen alloys, as opposed to copper-titanium alloys, rise in a

capillary tube or infiltrate a porous ceramic. Three possible phenomena that could cause the observed differences are discussed.

Table 1 Experimentally Measured Contact Angles

Time (Secs)	θ Degrees	
	Cu-8.5 w/o Ti at 1120°C	Cu-3 w/o O at 1300°C
1	126.1	34.4
50	121.9	34.4
1100	72	-
94000	14.3	-

Titanium Preconditioning of Alumina

Introduction

Interest

The mechanical properties of alumina-reinforced aluminum matrix composite materials especially high stiffness, strength, fatigue resistance, excellent wear resistance, low thermal expansion, and creep resistance, make this material system very attractive for industries such as automotive and aerospace. As components fabricated from these materials become less expensive to produce, the interest and demand for these materials will only increase. Of all of the available reinforcement materials and processes for the manufacture of aluminum-matrix composites, liquid-state processing of Al_2O_3-Al composites is the most cost-effective approach [16, 17].

Aluminum-matrix composites currently are widely manufactured through powder metallurgical routes; however, liquid-state processing of these materials may prove to be more cost-effective. Liquid processing does not involve comminution cost associated with powder metallurgical techniques. Liquid-state processing consists of relatively few steps

as compared to powder metallurgy (comminution, mixing, injection, and sintering). The possibility of near-net shape fabrication is an advantage of solidification processing due to difficulties associated with machining materials of this nature.

The cost-effective liquid-state production of alumina-reinforced aluminum-matrix composite materials has been hindered by interfacial and wetting characteristics of the alumina-aluminum mating surfaces. These composite materials are currently produced by techniques such as the Lanxide process, an in-situ oxidation process, powder processing, or ceramic-metal slurry casting.

The success of these composite materials is dependent upon the viability of the interfacial reaction zone that forms between the metal and ceramic during processing. The reaction zone should be strong and free of brittle intermetallic phases [18]. These characteristics in composite materials increase both fracture strength and fatigue life [18].

Approach

To develop a high bond energy interface between the metal and ceramic, chemical bond formation with an associated electronic structure change must occur at the interface. In the Al_2O_3-Al system, such a bond is thermodynamically feasible, but unfortunately not experimentally observed [19]. Inadequate interfacial formation can be attributed to the following attributes of the Al_2O_3-Al interface: a) low driving force for the reaction

between liquid aluminum and aluminum oxide, b) presence of an oxide layer on the liquid aluminum, which is protective and acts as a barrier to intimate contact, and c) the wetting kinetics are too sluggish for practical processing.

Titanium is known to react with the surface of aluminum oxide to generate a favorable interfacial gradient with respect to both stress and composition [20, 21, 22]. The driving force for wetting is sufficiently large to develop complete coverage of the alumina surface, as well as to form both titanium-rich and aluminum-rich interfacial reaction products [20, 21, 22]. Titanium supports multiple oxidation states. The inherent defect structure of titanium oxides allows the interface to tolerate large degrees of non-stoichiometry and to obtain favorable composition and stress gradients at the metal-ceramic interface [15, 23]. The defect structure of titanium oxides allows rapid diffusional transport at the interface, and consequently, rapid bonding between the metal and ceramic. Rapid bonding between the metal and ceramic potentially can significantly reduce the required processing time.

Chemical vapor deposition has been shown to be an effective method to metallize ceramic surfaces for various applications. In this program, a commonly employed chemical vapor deposition (CVD) technique known as pack cementation was used to precondition an alumina substrate material. The salient features of the CVD process were studied, and the behavior of the titanium-based CVD coating when in contact with molten, un-alloyed aluminum were investigated. The CVD coating has been identified as a two-

phase coating consisting of α-Ti and Ti_3Al. An activation energy and extrinsic rate constants for the pack cementation coating process were determined. The activation energy and rate constants are close to those reported by various authors for the formation of Ti_3Al on Al_2O_3, by both CVD methods and solid-state diffusion couples. The agreement in rate constants and activation energies has lead to the conclusion that growth of the CVD coatings is controlled by solid-state diffusion mechanisms, as will be further explained in the Results and Discussion section of this report.

Auminum-Alumina Interface

The Al-Al_2O_3 material system presents some interesting challenges with regard to liquid-metal processing of Al_2O_3 reinforced aluminum matrix composite materials. Liquid aluminum does not extensively wet alumina, nor does adequate interfacial formation occur when the liquid aluminum is brought into contact with alumina.

It has been found that the wetting of ceramic materials and graphite by liquid aluminum is controlled primarily by the oxide layer on the surface of the liquid aluminum. At experimentally obtainable oxygen partial pressures, most liquid metals will form an oxide layer which is usually a few angstroms thick [19, 24]. At 1300°Can oxide layer will form which is thermodynamically stable on liquid aluminum at oxygen partial pressures as low as 10^{-34} atmospheres. Formation of this oxide layer at the melting point of aluminum, 660°C, will occur at oxygen partial pressures as low as 10^{-25} atmospheres [19, 24]. This

oxide layer on aluminum is protective in nature. Laurent, *et al* [25] have similarly associated problems with formation of aluminum-ceramic interfaces with the presence of a protective oxide layer on liquid aluminum.

The wetting of ceramics in contact with liquid aluminum has been shown to exhibit a time dependence [19, 24-27]. These researchers have found that the contact angle of liquid aluminum in contact with various ceramics varies with respect to isothermal holding time. The studies cited above have related the wetting of various ceramics by aluminum to the stability (both physical and thermodynamic) of the oxide layer present on liquid aluminum. Chidambaram, *et al* [19, 24] have reported an incubation time prior to wetting of ceramic materials by liquid aluminum at temperatures below 950°C.

Wetting of ceramic materials by liquid aluminum has been observed to occur above a transition temperature [24, 26]. This temperature has been related to the destabilization of the oxide layer on the molten aluminum.

Achievement of adequate wetting has often been found to be associated with some degree of reactivity of the metal with the substrate, or with a reduction in the tenacious nature of the oxide film present on the molten metal [17]. To realize a high integrity bond in the liquid processing of aluminum matrix composites, the oxide layer must be removed, or at least destabilized. Several attempts have been made to produce chemical alterations of the materials systems to overcome the poor wetting characteristics of certain ceramics in contact with molten metals [17].

To achieve wetting the surface of the reinforcement or the matrix can be altered in such a way as to enhance chemical reactions at the interface or disrupt the oxide layer at the surface of the liquid metal. These methods include pretreatment of the ceramic surfaces, alloying additions to aluminum, and coatings applied to the surfaces of the ceramics

Alloying additions which promote reactivity of the metal with the reinforcement, such as, titanium, lithium, manganese, molybdenum, magnesium, and silicon have been shown to lower the wetting angle [17, 19, 24, 27]. Other alloying additions which do not promote reactivity of the metal with the reinforcement, but modify the oxide layer on the liquid metal also are effective in improving the wetting behavior. Additions of calcium, sodium, magnesium, and lithium, in aluminum are known to decrease the wetting angle through alteration of the oxide film [17, 28].

Coatings can also be applied to the surface of the reinforcement to improve wettability. These coatings are usually either metallic in nature or some sort of fluxing agent. Metallic coatings are used to react with the matrix or reduce the oxide layer on the surface of the metal. Fluxing agents such as K_2ZrF_6 destabilize the oxide layer. Most coatings that react with the matrix below 900°C are active primarily because they disrupt the oxide layer on the surface of the metal. Magnesia coatings on Al_2O_3 have been used to increase the wettability by liquid aluminum [17].

Titanium-Alumina Interface

Titanium in contact with alumina exhibits superior wetting behavior as compared to aluminum. The driving force for interfacial phase formation for titanium in contact with alumina is sufficiently large to develop complete coverage of the alumina reinforcement material. Titanium-rich and aluminum-rich reaction products result. The inherent defect structure associated with the oxides of titanium allows for rapid diffusional transport of metal cations through the subsequent reaction layers, and thus rapid bonding of titanium-containing alloys to alumina. The defect structure of certain oxides of titanium allows large degrees of non-stoichiometry at the interface. The TiO lattice is know to be very rich in defects. Up to 35 percent of the lattice sites in TiO could be lattice defects [29]. Therefore, alumina in contact with titanium reacts to form interfaces which are favorable with respect to gradients of stress and composition. Titanium aluminides have been found to be chemically compatible with Al_2O_3, and the coefficients of thermal expansion (CTE) of titanium aluminides and Al_2O_3 are quite similar, thus minimizing residual stresses resulting form cooling from the processing temperature [29].

Li *et al* [21] have proposed the following interfacial layer sequences, $Al_2O_3/TiAl/Ti_3Al/\alpha/\beta$-Ti and $Al_2O_3/Ti_3Al/\alpha/\beta$-Ti, for thin and thick titanium end members, respectively. Figure 12 is the isothermal section of the Ti-Al-O system proposed by Li *et*

al at 1100°C, with diffusion paths for thick and thin titanium end-members marked on the section. Li *et al* [21] reported initial formation of TiAl in the beginning, which reacts with the unsaturated α-Ti(O) solution of composition $Ti_{8/3}O$ according to the following reaction scheme:

$$12\ Ti + Al_2O_3 \rightarrow 3\ Ti_{8/3}O + Ti_3Al(O) + TiAl(O) \qquad 2$$

$$3\ Ti_{8/3}\ O + TiAl(O) \rightarrow 3\ Ti_2O + Ti_3Al(O) \qquad 3$$

Adding equations (12) and (13):

$$12\ Ti + Al_2O_3 \rightarrow 2\ Ti_3Al(O) + 3\ Ti_2O \qquad 4$$

Actual experimental values for the mean compositions for thin titanium end-members as reported by Li *et al* are:

$$10.2\ Ti + Al_2O3 \rightarrow 7.9\ Ti_{0.680}Al_{0.238}O_{0.082} + 7.29\ Ti_{0.662}Al_{0.016}O_{0.322} \qquad 5$$

Hatakeyama *et al* [30] have observed the formation of a reaction product between alumina and titanium annealed at temperatures ranging from 900°C to 1200°C. The reported interfacial reaction product of the titanium-alumina diffusion couples contained two distinct regions. Region I lies adjacent to the titanium and is single phase identified as Ti_2Al or Ti_3Al. Region II lies adjacent to the alumina, has been identified as TiAl.

DeKock *et al* [31] have conducted diffusion couple experiments using titanium-alumina diffusion couples held at 1100°C. The interfacial sequence is β-Ti/α_2-(Ti,Al)/α_2-Ti_3Al/γ-TiAl/Al_2O_3. This interfacial structure is in agreement with the isothermal section of the Ti-Al-O constitution diagram presented in their publication, which is given in Figure

13. These researchers have stated that composites produced of titanium and alumina are unstable and would not survive high temperature applications.

Ohuchi *et al* [32]have observed the reduction of Al_2O_3 by titanium and have characterized electronic structure changes at the titanium-alumina interface. The reduction of Al_2O_3 by titanium was characterized by changes in the oxygen 1s and titanium 2p photoemission spectra peaks. Spectral analysis revealed that oxygen atoms near the surface of the Al_2O_3 became more electron rich. The deposited titanium donated charge to the Al_2O_3 substrate. Reduction of aluminum-oxygen bonds was detected to provide the formation of a reduced species of aluminum, Ti_3Al.

Chemical Vapor Deposition Technology

A commonly used technique for metallizing ceramic surfaces is chemical vapor deposition (CVD). Chemical vapor deposition is also commonly used to coat metals with protective coatings for corrosion resistance, wear resistance, and surface hardening for tool and die applications [33-35]. Chemical vapor deposition coatings also have been used to limit the extent of chemical reaction between ceramic reinforcement and matrix in the production of composite materials [31].

A commonly used CVD technique is know as pack cementation. Cockeram, *et al* [33] and Bianco, *et al* [35] have presented an extensive explanation of the pack cementation process

Partial pressure-temperature relationships can be determined through an approach utilizing Gibbs free energy minimization of the various species in the system. The thermodynamic calculations are quite involved for simple systems, and become exceedingly difficult for systems in which several elements are interacting. Computer programs such as SOLGASMIX can be used to determine the partial pressure-temperature relationships for the gaseous species present in the pack. The thermodynamic stability of the halide activator determines the partial pressures of the halide species. Low stability activators result in high partial pressures for the elements of the master-alloy, and high fluxes of the elements of the master-alloy in the gas phase [33].

The pack cementation process, like all diffusion phenomena, is driven by activity gradients. Gas phase diffusion within the pack is driven by a partial pressure gradient for each of the volatile halide species [35]. In either of the two cases mentioned above, the thermodynamic activity of the elements of the master-alloy at the surface of the substrate is lower than the respective elements activity in the pack [33, 35]. It is this activity gradient which drives gas-phase diffusion of the volatile species within the pack to the surface of the substrate [33, 35]. The activity gradient between an element in the pack and the surface of the substrate is maintained by solid-state diffusion/reactions of the elements of the master-alloy with the surface of the substrate [33].

The reaction in which the largest drop in chemical potential of the element to be deposited occurs is the rate limiting step. The rate limiting step determines the overall rate

of the pack cementation coating process [33, 35]. Gas-phase reactions and interfacial reactions are not expected to rate determining steps [33, 35-42]. If solid-state diffusion is the rate-determining step, the growth kinetics are similar to that of a scale forming during the oxidation of a metal. If this is indeed the case, Wagner scaling theory can be used to describe the parabolic growth of the coating layer [23, 54]. If the flux of the elements of the master-alloy supplied to the substrate surface by the gas phase is sufficient, solid-state diffusion is the rate-limiting step, and growth kinetics of the layer should not depend on the type of activator used [23]. In systems in which highly stable activators are used, the growth kinetics of the CVD layers is controlled by gas phase diffusion in the pack [23]. Work on aluminizing of nickel and titanium alloys has shown that less stable activator result in faster growth kinetics [23, 53, 48, 51].

Cockeram *et al* [23] have reported parabolic thickening of titanium-silicide layers on pure titanium substrates produced by the described pack cementation technique. Activation energies and intrinsic rate constants for each titanium-silicide phase for the pack cementation process were calculated and were found to be in agreement with those obtained from solid state diffusion couples of pure titanium and single crystal silicon wafers. In both solid-state diffusion couples and pack cementation samples the growth of the titanium-silicide layers exhibited parabolic thickening kinetics. Cockeram *et al* [23] thus concluded that the growth of titanium-silicide layers by the pack cementation method

is controlled by solid-state diffusion of the elements of the master-alloy through the layer to the surface of the substrate.

Experimental Techniques

This section discusses two main experimental procedures. The first portion of this section discusses the chemical vapor deposition (CVD) of titanium onto alumina. These experiments were performed to gain an understanding of the kinetics of the CVD coating process, as well as to determine the most appropriate CVD coating parameters to produce titanium-coated alumina substrates for subsequent immersion experiments

The second portion of this section discusses the immersion studies in which alumina substrates coated with titanium, CVD and PVD, were immersed into molten aluminum in open air, under a layer of molten (Na,K)Cl . The open-air immersion studies were conducted for various lengths of time, ranging from no holding time to holding times of 300 seconds, for preconditioned substrates, and as long as 9.0 kiloseconds (2.5 hours) for non-preconditioned substrates. The open-air immersion studies were conducted at temperatures ranging from 700°C to 1000°C

Materials

Alumina was chosen as the reinforcement material to be investigated in this study. This material is readily available at reasonable cost from a variety of sources. For this investigation AD-998 α-alumina plates, 114 mm x 114 mm, were obtained from Coors Ceramic Company. Aluminum oxide preforms containing 30 percent porosity were used for the later portion of this investigation to determine the infiltration behavior of molten

aluminum in preconditioned porous materials. For the CVD experiments, titanium powder, (99.5% pure, -325 mesh), was obtained from Cerac Incorporated. Hydrogen chloride gas was chosen as the activator specie for the CVD experiments. A mixture of high purity hydrogen chloride (14.80 molar percent) and electronic grade argon produced by Scott Specialty Gases served as the activator source. High purity argon mixed with 5 molar percent hydrogen from General Air Service and Supply was used to backfill the CVD reaction chamber. Aluminum granules, (99.9% pure, 2mm to 10mm diameter) from Aesar were used as the material for molten aluminum immersion experiments. A layer of molten (Na,K)Cl was maintained above the molten aluminum to destabilize the oxide layer.

Chemical Vapor Deposition Experiments

A commonly employed chemical vapor deposition (CVD) method known as pack cementation was exploited in this investigation. This process involves heating the substrate to be coated in a pack containing titanium and a halide activator. Titanium reacts with the halide activator to form titanium-halide vapors such as $TiCl_2$, $TiCl_3$, and $TiCl_4$. These titanium-halide vapors diffuse through the intrices of the pack to the surface of the alumina, react with the surface of the alumina, and then deposit as metallic titanium.

To determine the feasibility of the chemical vapor deposition process a thermodynamic evaluation of the system was performed. The public domain computer program 'SOLGASMIX' was manipulated to estimate the thermodynamic activity of the various gaseous species at temperatures ranging from 727°C to 1427°C. This program determines the partial pressures of the gas species through a Gibb's free energy

minimization approach. From the results of this analysis, the optimal coating temperature range was determined. Chemical vapor deposition by the chosen activator is feasible when the partial pressures of the titanium-containing transport species are both one order of magnitude greater than that of the other reactive species, and greater than 10^{-5} atmospheres. For this investigation, hydrogen chloride and sodium chloride were considered as possible transport species. Figure 14 is a plot of the temperature-partial pressure relations for the pertinent species for both the hydrogen chloride and sodium chloride activated atmospheres.

Based upon the results of the thermodynamic analysis, preliminary CVD experiments were conducted in sealed quartz ampoules. An AD-996 alumina substrate and titanium powder were loaded into a quartz ampoule which had been sealed on one end. The partially sealed ampoule was then attached to a vacuum system. The ampoule was then evacuated and backfilled with high purity argon. The evacuation and backfilling process was then twice repeated. The ampoule was then evacuated and hydrogen chloride gas was then put into the ampoule. The pressure of the hydrogen chloride gas at room temperature was such that the ampoule would be at slightly positive pressure at the reaction temperature. For the experiments in which sodium chloride was chosen as the activator specie, the procedure were similar to that established for the hydrogen chloride activated experiments, except that crystalline sodium chloride was added simultaneously with the titanium powder. In both types of experiments the titanium-to-chloride molar ratio was maintained at 100:1.

The sealed ampoules were heated within a Marshall tube furnace in an open-ended mullite tube, for various reaction times and temperatures. Upon completion of the

experiment, the quartz ampoules were allowed to furnace cool to ambient temperature. The ampoules were then removed and the substrate removed for subsequent analysis.

Although coating of titanium onto alumina was feasible in the quartz ampoules, the experimental reliability of the quartz ampoules was too low to produce specimens for the entire study. Approximately 50 percent of the ampoules ruptured or developed flaws which lead to contamination of the atmosphere in the ampoule, during the time at temperature. Based on this probability of failure, and the relatively poor nature of the sodium chloride activated coatings as compared to the hydrogen chloride activated coatings, a more reliable CVD reaction chamber was constructed for the purpose of conducting hydrogen chloride activated CVD experiments.

The CVD reaction vessel consisted of a mullite tube with a compression-fit viton seal connected to an on-line gas train, vacuum system, and thermocouple. A schematic diagram of the CVD reaction vessel is given in Figure 15.

Alumina substrates for the following CVD experiments were cut into 20-by-40 mm sections. The substrates were prepared for the CVD experiments by washing in nitric and hydrochloric acid to remove residual debris and metal scratches resulting from the cutting operation. After acid washing, the substrates were rinsed in tap water then in ethanol, and dried using a hot air gun.

The cleaned substrates were packed in titanium powder contained within an alumina boat. The substrates were completely encased in titanium powder. Once the pack had been loaded into the furnace, the chamber was then sealed and a series of evacuation and backfilling steps were employed. When the chamber had reached a temperature of approximately 250°C, the chamber was evacuated and a mixture of HCl and argon was introduced. The pressure was continuously maintained at a positive pressure of

approximately 10 psi throughout the entire heat-up cycle by venting excess pressure through a three-way ball valve as the temperature of the chamber increased. A constant positive pressure was maintained during the entire coating time. As the reaction chamber cooled to ambient temperature the mixture of argon and hydrogen was added to maintain the positive pressure.

Upon removal from the titanium pack, the excess titanium powder adherent on the surface of the substrate was removed by socially vibrating the substrates in ethanol. Any titanium remaining on the substrate thereafter was remove by rubbing the ethanol soaked substrate with latex-gloved fingers. A final ethanol rinse and hot air drying concluded the sample preparation. The CVD-coated alumina substrates were characterized using X-ray diffraction (XRD), and energy dispersive X-ray spectroscopy (EDS) attachment to the Scanning Electron Microscope (SEM). A JEOL JXA 840 SEM with a Tracor Northern EDS spectrometer, and a Rigaku rotating anode diffractometer, using copper Kα radiation of 15.4179-nm wavelength were used for this purpose.

The thickness of the CVD coatings was measured using a Tencor Alpha-Step profiler. This measurement was obtained by tracing a diamond stylus over a step in the CVD coating. This step was created by masking half of the substrate with tape and immersing the unmasked portion in hydrofluoric acid. This process left a clean step in the CVD coating. After immersion, the substrate was immediately rinsed in water. Ethanol was then used to remove any residue left by the tape. Three traces were taken for each sample to calculate the mean and standard deviation of the thickness. Figure 16 is a schematic diagram of the substrate with the acid-etched step.

To obtain a value of the coating thickness which was representative of only deposition which occurred during the isothermal portion of the thermal cycle, the reaction

time was segregated into two portions, the isothermal holding time and the non-isothermal heat-up and cool-down times, and the contribution to the total thickness resulting from deposition in the respective sections were segregated from one another. To determine the extent of deposition during the non-isothermal portions of the thermal cycle, a coating experiment was conducted in which the thermal cycle consisted of only the non-isothermal portion of the thermal cycle. This experiment was specified to have a zero second isothermal holding time. For each temperature the coating thickness obtained from the zero second isothermal holding time samples was subtracted from the total coating thickness. This value was reported as the corrected thickness. The corrected thickness of the coatings was then plotted against time as well as the square root of time. The logarithm of the corrected thickness was plotted against logarithm of time for all coating temperatures. The slope of these plots was used to determine the order of the time-dependent thickening of the CVD coatings. The thickening of the CVD coatings exhibited a parabolic time dependence. Based on analysis of the order of the time dependent thickening, the corrected thickness was also plotted against square-root time. Parabolic thickening rates for three temperatures were calculated. An Arrehnious analysis was conducted to determine the activation energy for the formation of the entire CVD coating. The results of this analysis is presented in the results and discussion section of this thesis. The experimental matrix for the chemical vapor deposition portion of this study is summarized in Table 2.

Table 2 Chemical vapor deposition experimental matrix

time (ks)	610°C	procedure preformed 727°C	870°C
0	profilometry	profilometry	profilometry
3.6	profilometry	profilometry	profilometry
10.8	profil./XRD	profil./XRD	profil./XRD
18.0	profil./XRD	profil./XRD	profil./XRD
43.2	profil./XRD	profil./XRD	profil./XRD
64.8	profil./XRD	profil./XRD	profil./XRD

Immersion Experiments

To determine the wetting behavior of the CVD-titanium-coated alumina surface in contact with molten aluminum, a simple experimental approach was developed. CVD-coated Coors AD-996 alumina substrates were inserted into molten aluminum for various lengths of time and at various temperatures above the melting point of aluminum. Figure 17 is a schematic diagram of the immersion apparatus.

These experiments were conducted in open air. A molten layer of (Na,K)Cl was maintained above the molten aluminum to destabilize the oxide layer present on the aluminum. This salt was periodically added to the melt prior to immersion of each substrate.

The substrates were lowered to a position immediately above the molten aluminum and held there for a few seconds, then inserted into the melt. The holding time was necessary to allow the temperature of the substrate to increase such that the thermal shock upon entering the melt would be minimized. (Severe thermal shock caused the substrate to shatter when entering the melt). Upon withdrawal from the molten aluminum, the sample was held for a few seconds before being fully removed from the mullite tube. This procedure was followed to minimize thermal shock during cooling.

After immersion, the samples were washed in water to remove the residual salt layer. Cross-sectional analysis samples, as well as surface coverage samples were then prepared. The cross-sectional samples were mounted in a cold-curing low-viscosity epoxy, polished, and carbon-coated by vapor-depositing in preparation for SEM analysis.

Non-uniform wetting of the immersion specimens produced in open air was observed. The non-uniformity of the wetting behavior is believed to be a result of oxidation of the CVD coating at elevated temperatures immediately prior to immersion. To eliminate this effect, the immersion apparatus was moved into a controlled high purity

argon atmosphere glove box. The experimental matrix for the immersion tests conducted under controlled atmosphere is summarized in Table 3.

Table 3 Immersion experimental matrix

Immersion Temperature (°C)	Holding time (seconds)
950	10,30,60,120,150, 300
1080	0,10,30
1080 (uncoated substrates)	0,300,600,1800
1080 (coated substrates)	0,10,30
965 (porous preforms)	150, 300
1100 (porous preforms)	1800

The immersion specimens were characterized using energy dispersive X-ray spectroscopy (EDS) attachment to the Scanning Electron Microscope (SEM). A JEOL JXA 840 SEM with a Tracor Northern EDS spectrometer.

Results and Discussion

CVD Coating Characterization

Analysis of the X-ray diffraction patterns revealed that the CVD coating consisted of two-phases: α-titanium and titanium aluminide, Ti_3Al. Figure 18 is an X-ray diffraction pattern of a CVD-coated alumina substrate, coated at 729°C for 64.8 kiloseconds. Energy dispersive X-ray spectroscopy analysis in an SEM confirmed the existence of the two-phase microstructure in the as-deposited coating. Figure 19 is a backscattered electron image of the cross-section of a CVD coating produced at 870°C and a coating time of 64.8 kiloseconds. On this micrograph, three regions are present within the coating. The contrast of these regions is a manifestation of atomic number. Bright regions are areas rich in relatively high atomic number elements such as titanium. Areas rich in lower atomic number elements such as aluminum appear darker. EDS analysis determined the composition of the brightest region to be in the single phase a-Ti field. The composition of the intermediate region was within the two phase a-Ti and Ti_3Al field. The intermediate region appeared to be a mixture of α-Ti and Ti_3Al. The individual phases in this region were too small to clearly resolve and analyze by EDS technique. The composition of the darkest region in the coating was within the single phase Ti_3Al field. The highest titanium concentrations were present at the outer surface of the coating. Qualitative analysis of Figure 19, with respect to atomic number contrast, demonstrated the relative positions of the various phases in the coating. The titanium concentration decreases to a constant value as the substrate-coating interface was approached. Figure 20 is a schematic diagram of a proposed concentration profile for titanium and aluminum across the coating-

substrate interface. The compositions shown on the schematic represent α-Ti, two phase α-Ti and Ti_3Al, and Ti_3Al. Of the coating produced, only the coatings produced at 870°C and an isothermal holding time of 64.8 kiloseconds were thick enough to quantitatively by EDS. The diagram shown in Figure 20 is an estimation of the aluminum and titanium concentration profiles based upon the backscattered electron image shown in Figure 19. Figure 21 is a copy of the titanium-rich end of the Al-Ti phase diagram as presented by Murray [43]. To determine the progression of the coating process, the intensity of the titanium and titanium aluminide peaks was analyzed. To account for variations in the reported intensity of a given peak from one X-ray diffraction experiment to another, the intensity of the peaks was normalized to that of one of the prominent Al_2O_3 peaks. Analysis of the intensity of the Ti (101) peaks and Ti_3Al (201) peaks with respect to the Al_2O_3 (104) peak was used to track the phase changes as a function of isothermal holding time and coating temperature. Figures 22 through 25 are X-ray diffraction patterns from the 870°C specimens with the peaks of interest labeled. The ratio of the intensity of the Ti (101) peak to the intensity of the Al_2O_3 (104) peak increased with increasing coating temperature. The ratio of the intensity of the Ti_3Al (201) peak to the intensity of the Al_2O_3 (104) peak also increased with increasing coating temperature. Figures 26, 27, and 28 are intensity-coating time relations for the peaks of interest. If the data point corresponding to 64.8 kiloseconds for the 727°C in Figure 28 is disregarded, the conclusion can be drawn that intensity of the Ti_3Al (201) peak to the Ti (101) peak with

also increases with increasing coating temperature. The Ti/Al_2O_3, Ti_3Al/Al_2O_3, and $Ti_3Al./Ti$ intensity relations are invariant with respect to isothermal holding time. Time invariant reaction layer thickness have been reported by Cockeram and Rapp [33]. In the study conducted by Cockeram, et al, the thickness of individual titanium-silicide layers was measured using optical microscopy techniques, whereas in the present study intensity ratios of certain peaks was used as an estimation of relative amounts of α-Ti and Ti_3Al.

Kinetic Analysis of Coating Thickening

To gain a better understanding of the CVD coating process, an investigation of the coating thickening kinetics was undertaken. Figure 29 is a plot of the effect of isothermal holding time on the thickness of the CVD coatings for temperatures of 610°C, 727°C, and 870°C. Table 4 is a summation of the experimental measurements of coating thickness and reaction time.

Table 4 Corrected thickness of CVD coatings

time	$(time)^{0.5}$		thickness (μm)	
(ks)	$(ks)^{0.5}$	610°C	727°C	870°C
0	0	0	0	0
3.6	1.90	-	0.37	2.04
10.8	3.29	0.13	0.69	4.41
18.0	4.24	0.06	1.03	6.51
43.2	6.57	0.26	1.88	6.71
64.8	8.05	0.20	1.73	10.87

Figure 30 is a similar plot as Figure 29, but plotted on a decade grid. The lines of Figure 29 can be fit to an equation of the form:

$$corrected\ coating\ thickness = k(isothermal\ holding\ time)^n \qquad 7$$

where n is the order of the time-dependence of the thickening and k is a constant. Taking logarithm of both sides of equation (7):

$$log\ (corrected\ thickness) = log\ (k) + n log\ (isothermal\ holding\ time) \qquad 8$$

Linear regression of the thickness data with respect to Figure 30 and Equation 8 has determined the slopes of the lines to be approximately 0.5, indicative of parabolic time-dependent thickening kinetics. Actual values of these slopes and correlation coefficients are given in Table 5.

Table 5 CVD coating thickening exponents for CVD coatings prepared at 610°C, 727°C, and 870°C.

Coating Temperature (°C)	Thickening Exponent	Correlation Coefficient
610	0.504	0.395
727	0.583	0.968
870	0.524	0.929

The corrected thickness measurement from the 610°C samples do not correlate well, unlike the corrected thickness data from the coatings produced at 727°C and 870°C. The poor correlation is due to the error in the thickness measurement. These coatings were much thinner than those produced at the higher temperatures, thus the error in the thickness measurement is a much larger fraction of the measured thickness. Based upon the thickening exponents and correlation coefficients, the time dependence of the CVD coating thickening was determined to be parabolic. Figure 31 is a linear fit plot of the corrected coating thickness versus the square root of time for CVD coatings prepared at 610°C, 727°C, and 870°C. The error bars represent a 95% confidence interval, or two standard of deviations of the thickness measurement. No error bars are shown for points were twice the standard of deviation was a smaller dimension than the size of the plotting symbol.

Parabolic growth of CVD layers of titanium-silicide coatings on metallic titanium substrates produced through a similar pack cementation technique was observed by Cockeram *et al* [33]. Tressler 1973 [22] and Hatakeyama 1986 [30] have also reported parabolic time dependent growth of Ti_3Al layers in solid-state diffusion couples.

An apparent reaction rate constant for the entire coating process, k, was calculated from the thickening kinetics data. An intrinsic rate refers to the growth of a single layer without influence from neighboring layers. The intrinsic rate constant is representative of the atomistic processes contributing to the formation of the single layer. An apparent rate refers to the growth of a layer with influences from the neighboring layers, through mutual consumption of the layer of interest and the neighboring layers [44]. The apparent reaction rate constant is representative of the overall coating process, deposition of elemental titanium and formation of titanium aluminide, not the true rate of deposition of elemental titanium. Due to the competing processes of titanium deposition and reaction of the as-deposited titanium with the alumina substrate, separate reaction rate constants for the deposition and formation of the intermetallic titanium aluminide could not be distinguished with this analytical technique.

An expression for the apparent reaction rate constant can be written as:

$$k = \frac{CVD\,coating\,thickness^2}{Isothermal\,holding\,time} \qquad 9$$

An Arrehnious-type activation energy analysis can be used to calculate the temperature dependence of the apparent reaction rate constant, k. The values of the apparent rate constant are in agreement with those reported by Tressler *et al* [22], as estimated from Figure 10 of that publication. The rate constants for each temperature are reported in Table 6.

Table 6 Apparent reaction rate constant, k, as a function of temperature for the CVD coating process.

Temperature (°C)	k (cm^2/s)	k Tressler *et al* [7] (cm^2/s)
610	1.4×10^{-14}	2×10^{-14}
727	5.5×10^{-13}	8×10^{-13}
870	2.3×10^{-11}	9×10^{-12}

The apparent rate constant can be expressed as:

$$k = k_o \exp(\frac{-Q}{RT}) \qquad 10$$

A plot of the logarithm of the reaction rate constant versus inverse absolute temperature can be used to calculate the activation energy of the overall coating process, Q. Figure 32 is a plot of the logarithm of the reaction rate constant versus inverse absolute temperature. The slope of the line on this plot indicates an activation energy of 219 $kJmole^{-1}$. Activation energies of 216 $kJmole^{-1}$ and 142 $kJmole^{-1}$ have been reported

for the growth of Ti_3Al layers in this system by Tressler *et al* [22] and Hatakeyama *et al* [30] respectively for solid state titanium-alumina diffusion couples. The values of the intrinsic rate constants and activation energies are in close agreement with those reported by Tressler *et al* [22] for solid-state diffusion couples consisting of α-Ti vacuum diffusion-bonded to alumina.

Cockeram *et al* [33] have used Wagner's parabolic scaling theory to model the growth kinetics of the titanium-silicide layers controlled by solid-state diffusion for layers in which less stable activators were used in the packs. In this investigation, the Wagner theory for a single-coating layer was used to model the growth of the Ti_3Al layer.

The assumptions used in this application of the Wagner theory are as follows:

1. Only the formation of Ti_3Al in the coating, deposition of elemental titanium is assumed to occur during the cooling portion of the thermocycle while the activity of the pack is constantly changing and the reduction in temperature retards the diffusional processes controlling the transformation of titanium to titanium aluminide.
2. Planar interfaces between the substrate and coating.
3. Isothermal coating at 870°C.
4. Vapor-phase deposition of titanium is much faster than growth of Ti_3Al.
5. Diffusion of titanium and aluminum through the Ti_3Al layer is rate controlling.

6. Ti_3Al is a stoichiometric line compound.

7. Equilibrium at the Ti-Ti_3Al and Ti-vapor interfaces exists.

8. The diffusion coefficients are invariant with respect to composition.

The following derivation has been presented by Cockeram *et al* [33] and has been adapted for this characterization study. The Wagner parabolic scaling theory describes the growth of a single layer-coating layer as:

$$k_r = \frac{C_{eq}}{2}\int_{a'_x}^{a''_x}\left(\frac{Z_M}{Z}\right)[D_M + Dx]d\ln a_x \qquad 11$$

where k_r is the rational rate constant in units of equivalents/cm*s, C_{eq} is the number of equivalents/cm^3 for the M_aX_b layer, a_x is the activity of the coating element, and D_M and D_X are the self diffusion coefficients of the elements of the metal in the oxide of the substrate and coating respectively. A practical rate constant, kp in units of cm^2/s, can be defined in terms of the thickness of the coating layer (ξ) as:

$$\xi^2 = k_p t \qquad 12$$

The relationship between the practical rate constant and the rational rate constant is:

$$k_p = k_r / C_{eq} \qquad 13$$

Based on the above equations and assumptions of invariant diffusion coefficients the growth of a single layer of Ti_3Al, with X=Ti, can be described as:

$$k_p = \int D(d\ln a_{Ti}) = D\int (d\ln a_{Ti}) \qquad 14$$

Assuming thermodynamic equilibrium at the Ti-Ti_3Al and Ti-vapor interfaces, and unity titanium activity at the Ti-Ti_3Al interface, for growth of a single layer of Ti_3Al

$$\int d\ln a_{Ti} = \ln(a''_{Ti} / a'_{Ti}) = [\ln 1 - \ln a'_{Ti}] = -\Delta G^{o}_{Ti_3Al} / RT \qquad 15$$

where R is the gas constant, T is the absolute temperature, and $\Delta G°_{Ti3Al}$ is the standard Gibbs energy of formation for Ti_3Al. The following expression describes growth of a single layer of Ti_3Al

$$k_p = -D(\Delta G^{o}_{Ti_3Al} / RT) \qquad 16$$

The standard Gibbs energy of formation of Ti_3Al is strongly dependent on the amount of oxygen in solution. The maximum solubility of oxygen in Ti_3Al is 11 atomic percent at 1100°C [21]. Calculations using the standard Gibbs energy of formation of Ti_3Al with no oxygen in solid solution and 11 atomic percent oxygen in solid solution were conducted to account for the undetermined amount of oxygen in the experimental coatings.

Calculations of the estimated layer thickness using the Wagner scaling theory were performed for coatings performed for coatings prepared at 870°C for an isothermal holding time of 64.8 ks (18 hours). Thermodynamic data for this material system published by Li et al [21] was given at 1100°C and was assumed to acceptable for

estimations of the thermodynamic values at 870°C. Diffusion data published by Dayanada [45] for average effective interdiffusion coefficients of titanium and aluminum in Ti_3Al determined form a diffusion couple consisting of Ti_3Al ($\alpha 2$) base alloy (Ti-25 Al 10 Nb-3 V-1 Mo) and pure nickel were used to acquire an order of magnitude estimation of the self diffusion coefficient of titanium in Ti_3Al. A summarization of the data used in the theoretical calculations is given in Table 7

Table 7 Data used in theoretical calculations of the Wagner scaling theory.

Data	Value	Reference
$\Delta G°_f$ (Ti_3Al, 11at%O, 1100°C)	68.3 kJ/mole	Li et al [6]
$\Delta G°_f$ (Ti_3Al), 0at%O, 1100°C)	18.4 kJ/mole	Li et al [6]
D Ti in Ti_3Al, 1100°C	10^{-10} cm^2/s	Dayananda [57]

The results of the theoretical calculations are reported in Table 8. The results indicate that the experimental coatings roughly fit the Wagner parabolic scaling theory. Several assumptions were made to come to this conclusion, some of which may not be representative of what is occurring experimentally, and the accuracy of the calculation for growth of Ti_3Al layers on Al_2O_3 by the pack cementation process is poor at best.

Table 8 Results of Wagner's theoretical growth calculations for growth of Ti_3Al layers on Al_2O_3 by the pack cementation process at 870°C, 18 hours.

Condition	calculated thickness (μm)
0 at% oxygen in solution	50.1
11 at% oxygen in solution	96.5
experimentally measured	10.9 (actual)

Based upon the agreement between the activation energies and rate constants of this study and that of Tressler *et al* [22], as well as upon the observations of Cockeram *et al* [33] regarding solid-state diffusion controlled thickening in titanium-silicide coatings produced through similar pack cementation processes, it can be concluded that the development of the CVD titanium coatings through the pack cementation method is controlled by solid-state diffusion mechanisms. These results suggest that Ti_3Al forms at the surface of the coating prior to continued deposition of titanium, and that diffusion of oxygen atoms and aluminum atoms to the exterior of the coating controls the formation rate of Ti_3Al. To maintain an activity gradient in the pack, solid state diffusion and reaction of the deposited element or alloy with the substrate must occur. Such a mechanistic approach has been presented by B.V. Cockeram *et al* and Bianco *et al* [33, 35]. In these studies it has been found that less stable activators produced coatings in which thickening kinetics were governed by solid-state diffusion

mechanisms. More stable activator species produced coatings exhibiting thickening kinetics controlled by volume diffusion [38, 35].

The conclusion can be drawn that the CVD coating was initially deposited as α-titanium. The alumina substrate reacted with the α-titanium CVD coating while the substrate was at temperature, producing Ti_3Al. Ti_3Al formation provided the necessary activity gradient in the pack, in turn allowing further deposition of α-titanium. Titanium reacted with aluminum ions from the alumina substrate to form Ti_3Al during the remainder of the coating process. It is hypothesized that the titanium concentration in the coating was insignificant during the isothermal holding time. However, titanium is thought to have been deposited during the ensuing period following the isothermal holding time, as the temperature of the pack was lowered. Consequently, the activity of the pack continuously changed, causing titanium deposition on the particles in the pack, chamber surfaces, and coating surface. As the temperature decreased, the solid-state diffusion processes occurring at the substrate-coating interface and throughout the thickness of the coating were hindered, limiting Ti_3Al formation. The result was a residual layer of α-titanium deposited on the exterior surface of the coating during cooling. This phenomena can be seen in Figure 19. The α-titanium is present on the exterior surface of the coating, but can not be seen near the substrate/coating interface.

Immersion Sample Characterization

Analysis of the cross-sectional immersion samples demonstrated the effectiveness of the CVD coatings in enhancing the wetting behavior of the alumina substrate material as compared to uncoated alumina. In all of the experiments conducted with preconditioned substrates, wetting of the substrate was uniform, whereas in the experiments conducted with uncoated substrates, any wetting observed was scant and non-uniform.

For the immersion studies, all of the alumina substrates and preforms were prepared using the pack cementation technique. The coating temperature was maintained at 727°C for an isothermal holding time was 64.8 kiloseconds (18 hours). Wetting of the preconditioned substrates was observed immediately upon immersion at 950°C and 1080°C. Wetting of uncoated alumina substrates was not observed at either temperature for holding times as long as 1.8 kiloseconds (0.5 hours). Figure 33 illustrates the effectiveness of the CVD coating in enhancing the wetting behavior of the alumina substrate material. Figure 33 a) is a secondary electron image of an uncoated alumina substrate immersed in molten aluminum at 1080°C for a holding time of 1.8 kiloseconds (0.5 hours). No as-solidified aluminum is present on the surface of the sample. The particles present are particles of residual $CaCl_2$. The surface of the uncoated sample dramatically differs from that of a CVD coated substrate shown in the secondary electron

image in Figure 33 b). The substrate in Figure 33 b) was immersed in molten aluminum at 1080°C for a holding time of 10 seconds. A uniform layer of as-solidified aluminum is present, below the immersion line, on the surface of this sample.

The surface analysis of the immersion samples did not produce useful information regarding the phase relations during the immersion process. To determine the phase relations during immersion, interfacial analysis of the immersions samples was performed. Figure 34 present SEM micrographs of the interface of a CVD-coated Al_2O_3 substrate immersed at 950°C with a 10-s holding time. Four phases can be identified on this micrograph, as seen on the backscattered electron image of Figure 34 b). The darkest region at the far left of the micrograph is the alumina substrate. The two intermediate phases are the remains of the CVD coating. The brighter of the two intermediate constituents adjacent to the alumina substrate has a composition corresponding to the two-phase region of α-titanium and Ti_3Al. The phase in contact with the as-solidified aluminum and Ti_3Al has the composition of the line compound α-$TiAl_3$. The phase on the far right of the micrograph is the as-solidified aluminum, containing less than one atomic percent titanium in solid solution.

When the holding time was increased, the intermediate phases became less prevalent. At a holding time of sixty seconds, the interfacial sequence is similar to that of the 10-s holding time sample. Figure 35 presents SEM micrographs of the interface of an immersion sample produced at 950°C with a holding time of 30 seconds. The brightest

phase in contact with the alumina substrate is also α-titanium and Ti_3Al. The composition of the next brightest phase corresponds to that of the two-phase region of $TiAl_2$ and α-$TiAl_3$. As-solidified aluminum with less than 1 atomic percent titanium is in contact with the remains of the CVD coating at the outer extremity of the interface.

Similar phase formation is seen in the samples immersed at 950°C for 60 seconds as was observed in the 30 second holding time samples, as seen in Figure 36.

At 950°C, extending the holding time to 300 seconds developed an interface consisting of as-solidified aluminum with no detectable titanium in intimate contact with the alumina substrate. This interface is shown in the SEM micrographs of Figure 37.

At an immersion temperature of 1080°C the wetting of the preconditioned substrate was observed immediately upon immersion. Figure 37 are SEM micrographs of a sample immersed at 1080°C with no holding time. Only sparse remains of the CVD coating are identifiable in the backscattered SEM micrograph of Figure 37 b). The remains of the coating are present as isolated titanium-rich precipitate particles in the solidified aluminum. Similar samples with holding times as long as ten seconds exhibited no residual titanium at the substrate interface or in the solidified aluminum. Figure 38 are SEM micrographs of sample immersed at 1080°C for ten seconds. Notice the absence of titanium-rich particles at the interface or in the solidified aluminum as seen in the backscattered SEM micrographs of Figure 38 b).

In all of the immersion experiments using titanium preconditioned alumina substrates dissolution of the CVD coating was observed. The titanium-rich phases present in the CVD coating were observed to react with the molten aluminum and form other aluminum-rich phases. Figure 39 is a copy of the aluminum-titanium phase diagram as presented by Murray [43]. As holding time was increased, a stable, Class I, interface between as-solidified aluminum and alumina was developed. A stable, Class I, interface between aluminum and alumina was one of the goals of this research.

Extension of the preconditioning treatment was conducted to determine the feasibility of producing Al_2O_3-Al composite materials. Porous alumina preforms were preconditioned using the pack cementation technique described in the Experimental Techniques section of this thesis. Figure 40 b) is a backscattered SEM micrograph of the cross section of a CVD coated preform immersed in molten aluminum at 1100°C for 1800 seconds. The darker areas are alumina. The lighter areas are aluminum with less than one atomic percent titanium.

The success of the immersion experiments using titanium preconditioned alumina porous preforms illustrates the utility of the titanium preconditioning technique for producing Al_2O_3-Al composite material. While titanium preconditioning through the pack cementation process is a viable way to enhance the wettability of aluminum oxide reinforcement material for liquid-state production of aluminum-matrix composite material, this process may be unfeasible for industrial applications. Hydrogen chloride activated

pack cementation requires the use of dangerous and corrosive gas species, which present special challenges with regard to upscalling of equipment. This study has shown that long processing times are required to prepare the reinforcement material. In addition to the long processing times required to prepare the reinforcement material, steps must also be undertaken to remove residual titanium powder from the reinforcement. At high coating temperatures the titanium powder sinters and bonds to the reinforcement. For these reasons the pack cementation process for titanium preconditioning Al_2O_3 reinforcement for liquid-metal processing of aluminum-matrix composite materials may have limited potential for industrial applications

Conclusions

Chemical vapor deposition of titanium onto the surface of alumina has been demonstrated to be feasible through the HCl activated pack cementation method. The typical two phase microstructure of the CVD coating has been identified as α-titanium and titanium aluminide, Ti_3Al. The thickening of the CVD coating exhibits a parabolic time dependence, and the rate of thickening of the CVD coatings has been shown to be controlled by solid-state diffusion mechanisms. The activation energy for formation of the entire coating has been determined as 219 $kJmole^{-1}$. The growth of the CVD Ti_3Al by the pack cementation process has been shown to roughly fit Wagner's parabolic scaling the for growth of a single layers.

CVD titanium preconditioning of alumina has been shown to enhance the wetting characteristics of alumina in contact with molten aluminum. A stable Class I interface between aluminum and alumina has been produced through immersion experiments using both planar alumina substrates and porous alumina preforms preconditioned by the pack cementation technique.

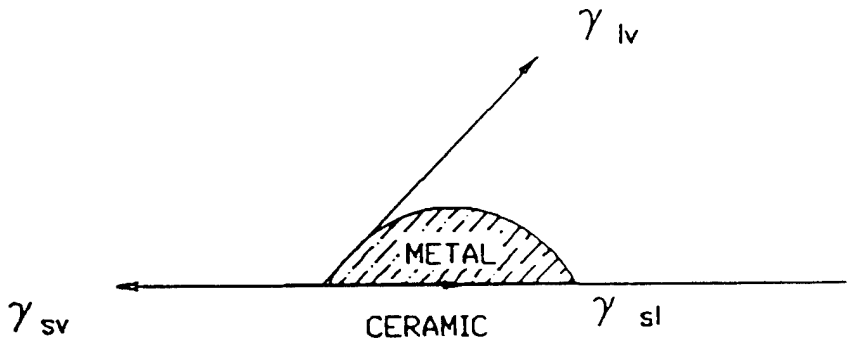

a) wetting

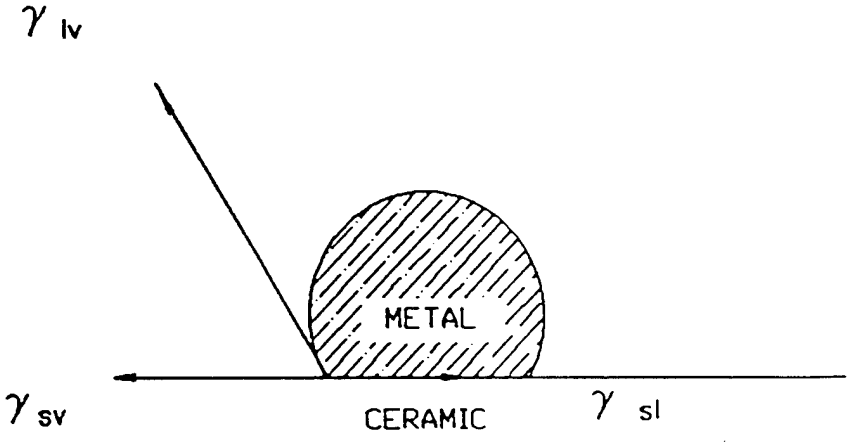

b) non-wetting

Figure 1 A schematic illustration of the wetting phenomena: a) wetting b) non-wetting

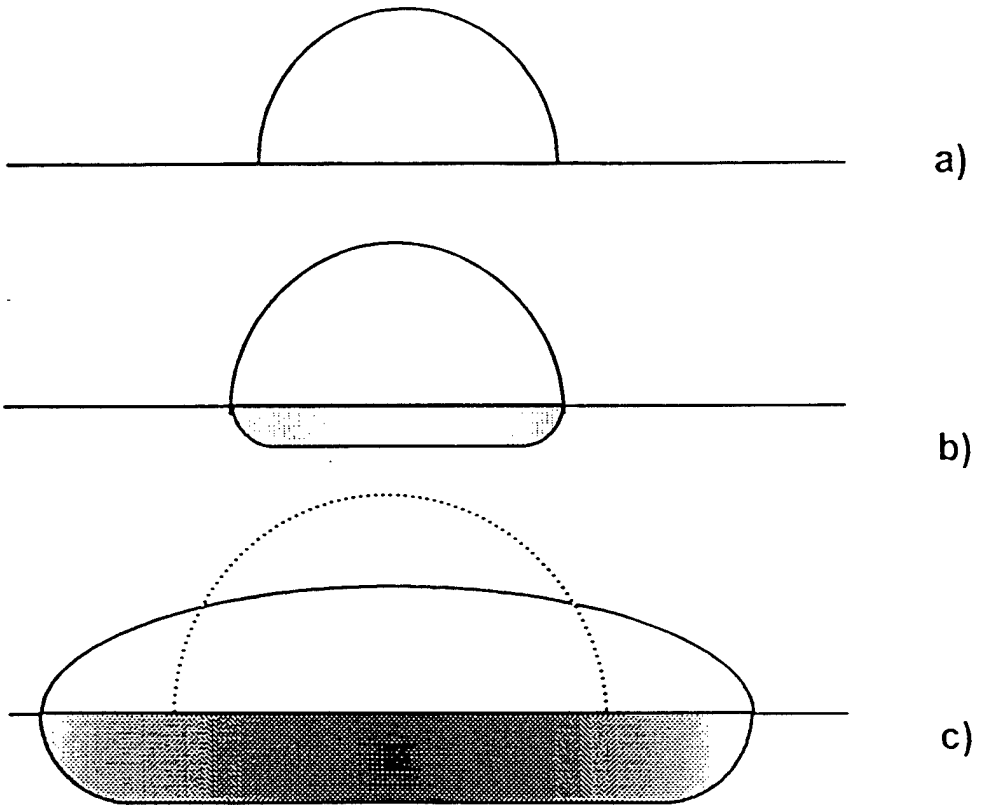

Figure 2 Schematic diagram illustrating the two stages involved in the spreading of a liquid drop: a) initial contact, b) Stage-I, and c) Stage-II

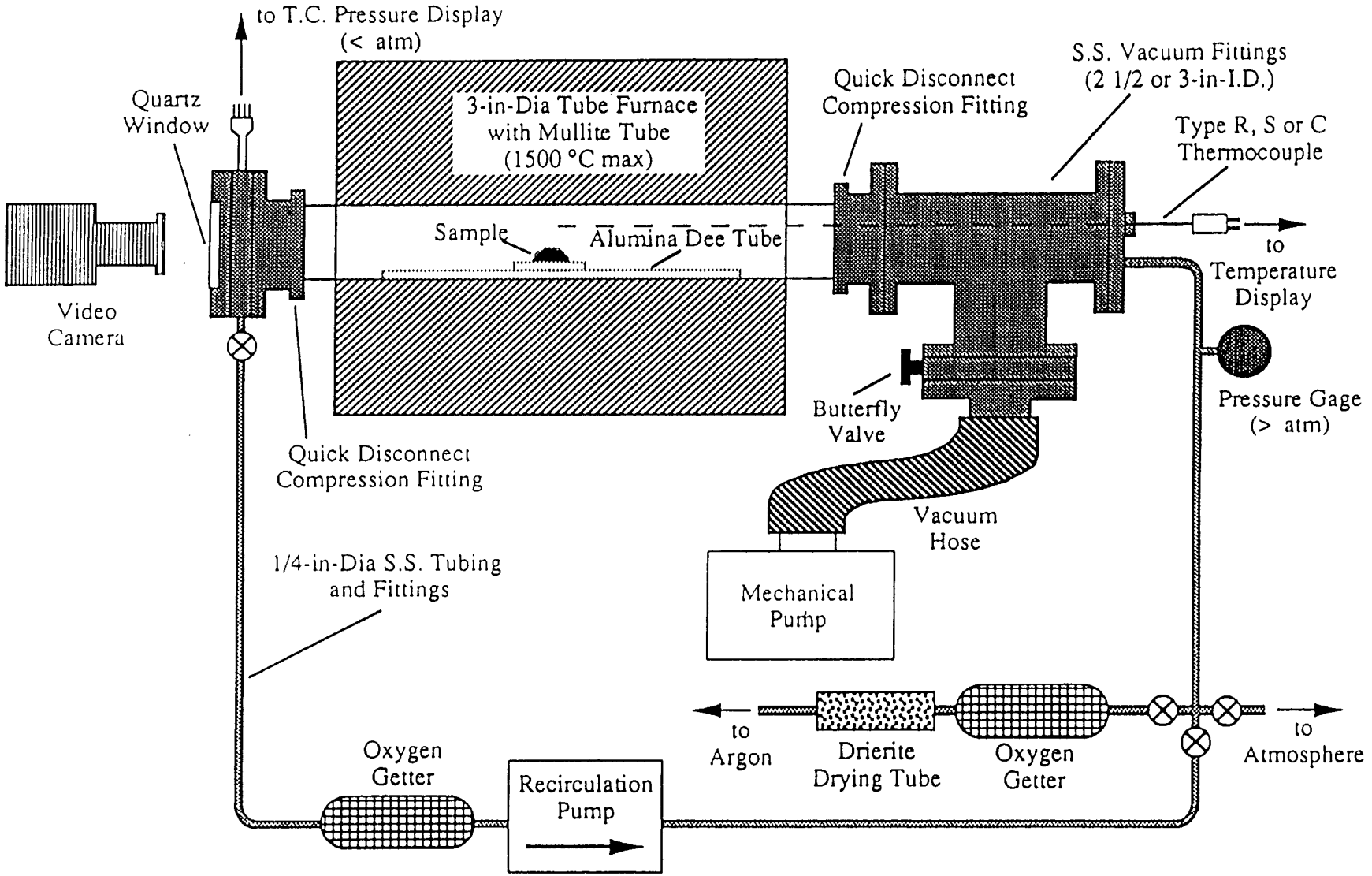

Figure 3 Schematic diagram of the apparatus used for measuring sessile drop diameters.

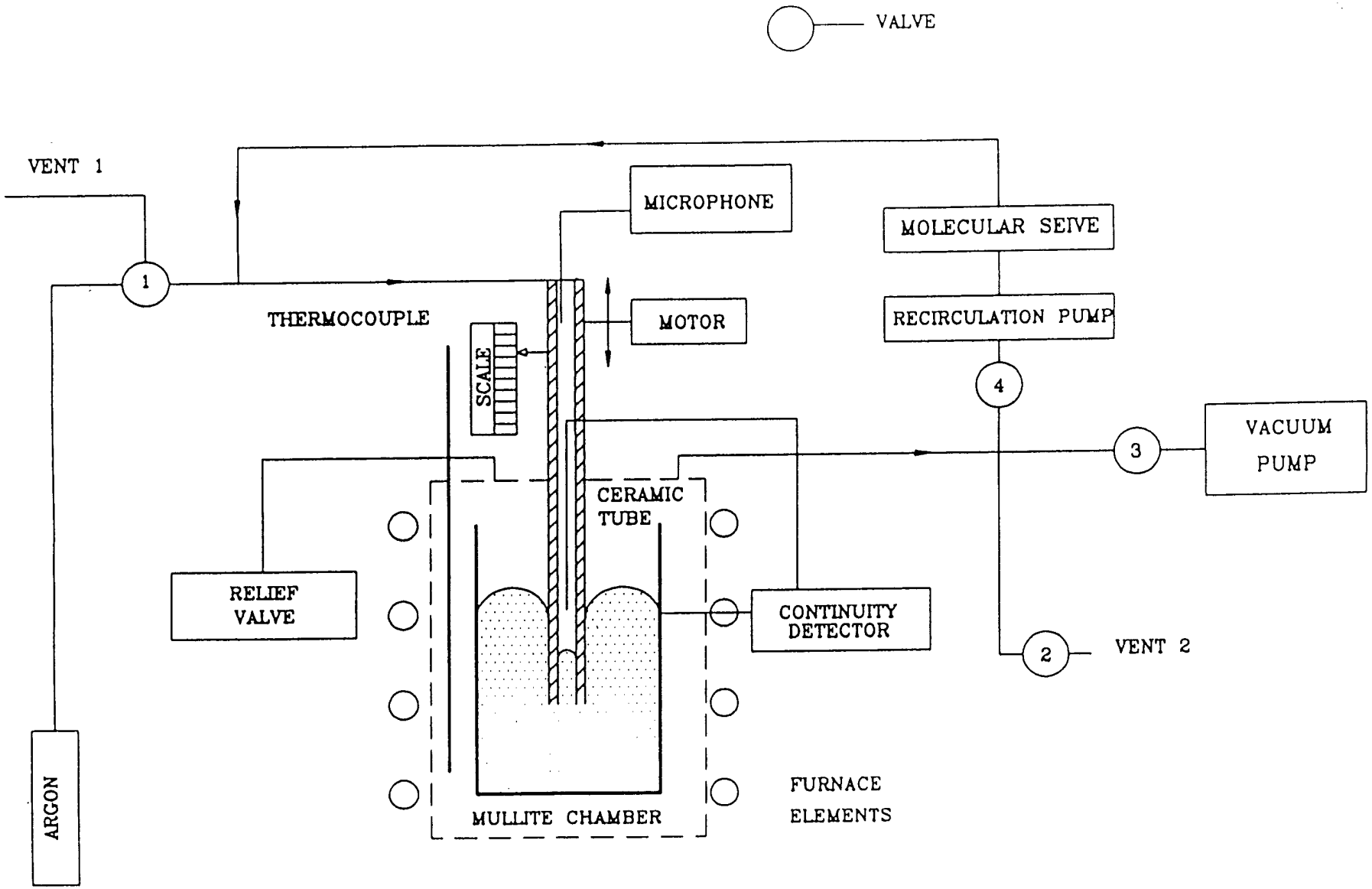

Figure 4 Schematic diagram of the apparatus used for measuring the capillary rise

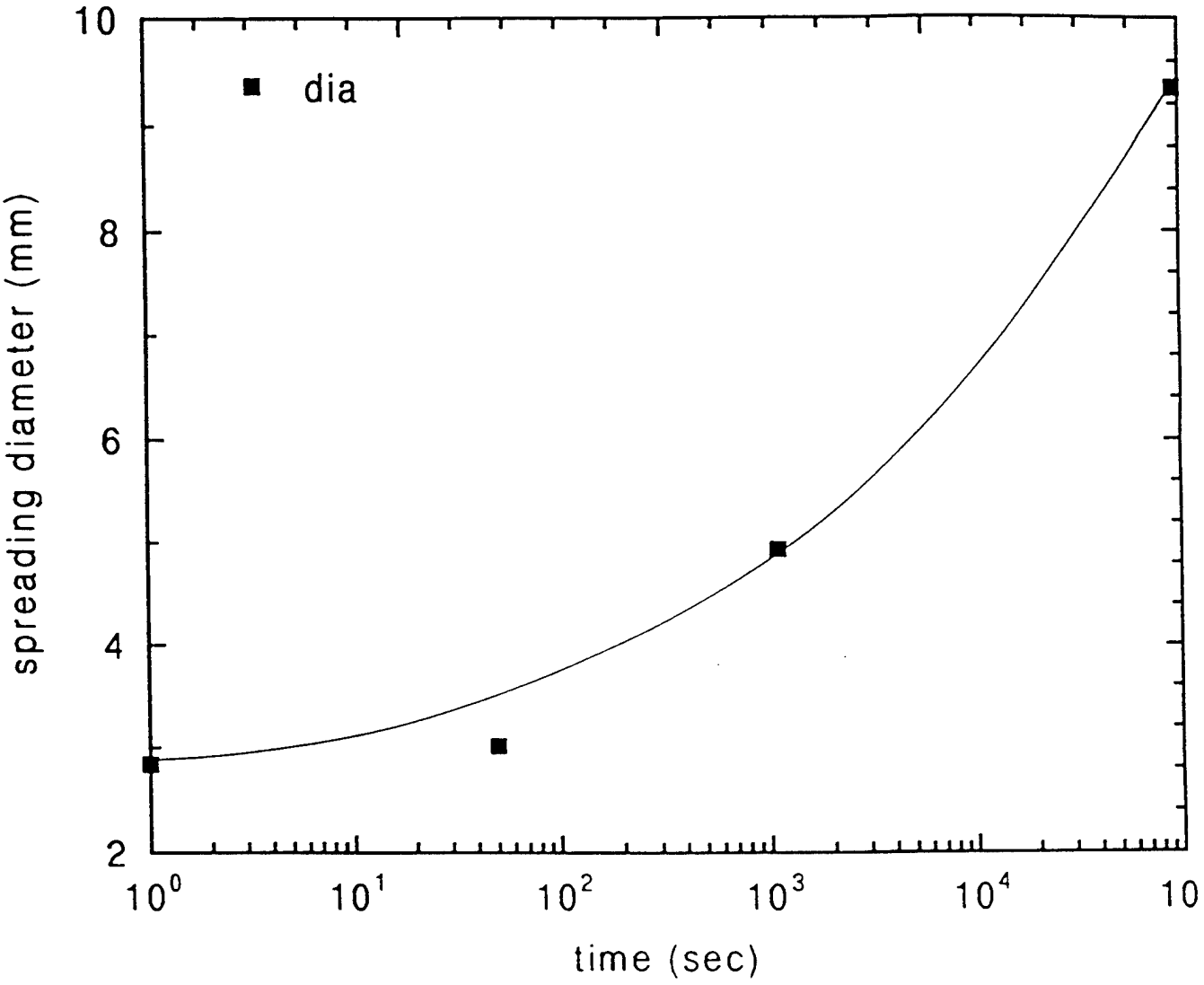

Figure 5 The diameter of the copper-8.5-w/o titanium drop spreading on alumina as a function of time

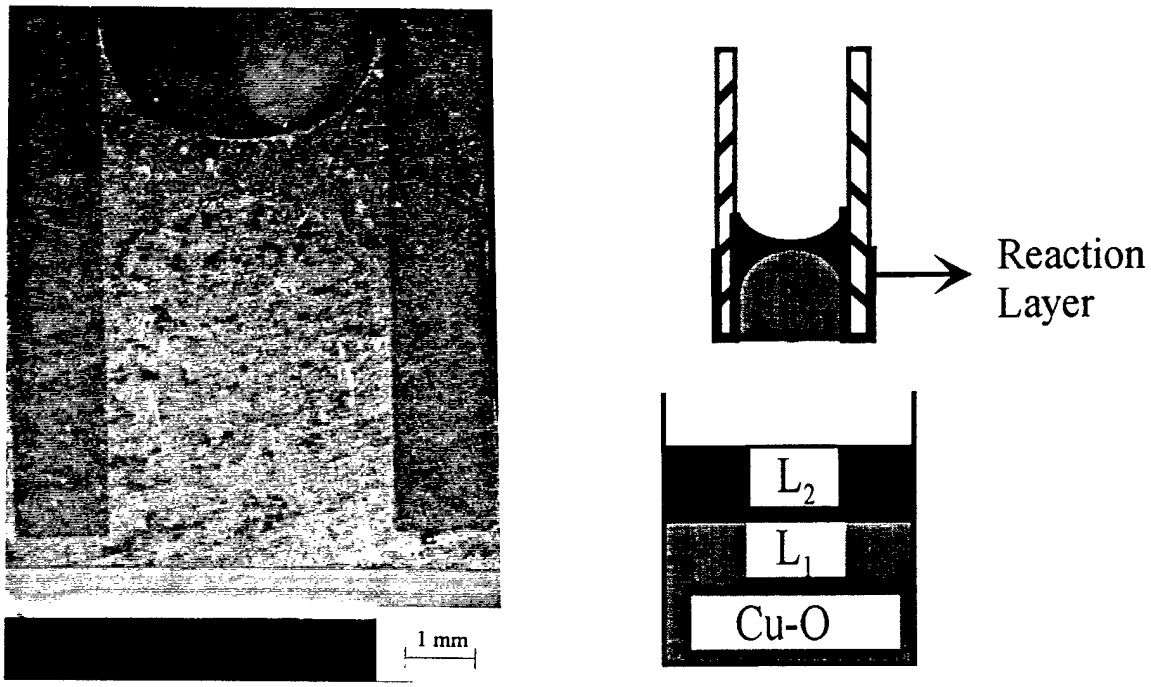

Figure 6 a) A cross-sectional macrograph of the alumina filter tube in contact with liquid copper 3-w/o oxygen alloy at 1300°C and b) a schematic diagram illustrating the liquid morphology.

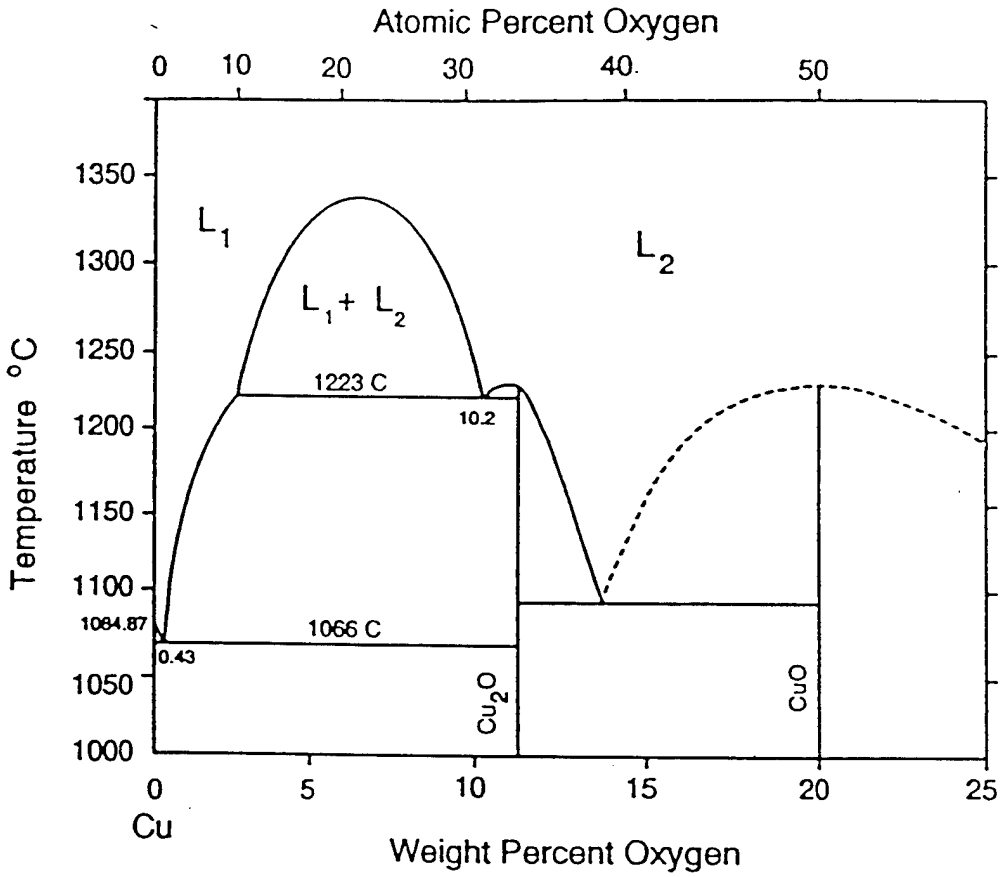

Figure 7 The Copper-Oxygen phase diagram [8]

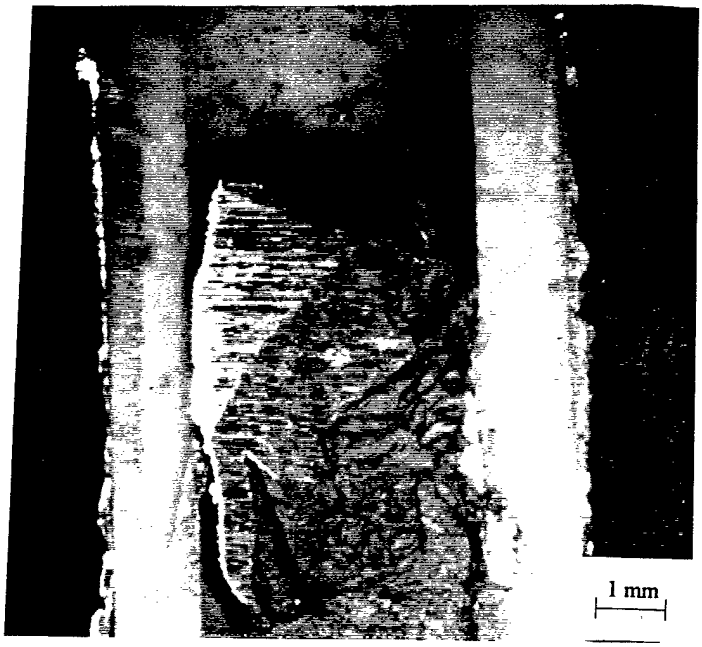

a

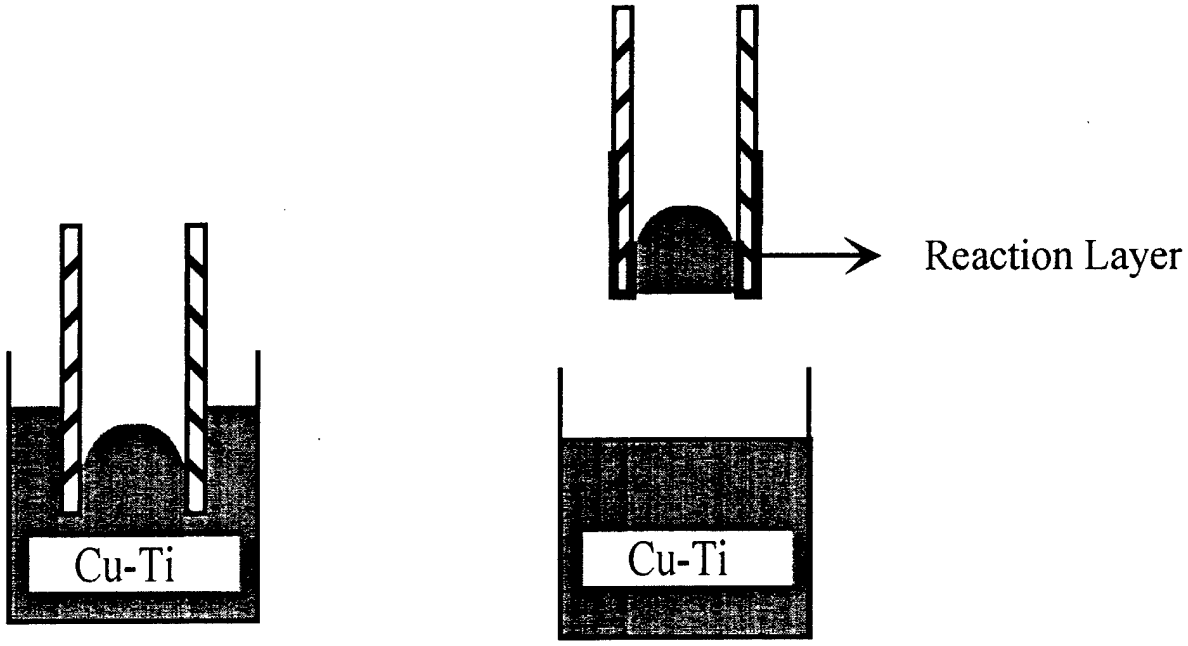

b

c

Figure 8 The liquid morphology when the alumina tube is immersed in copper 6-w/o titanium and withdrawn. a) cross-sectional micrograph, b) schematic diagram representing the immersed condition c) schematic diagram representing the withdrawn condition.

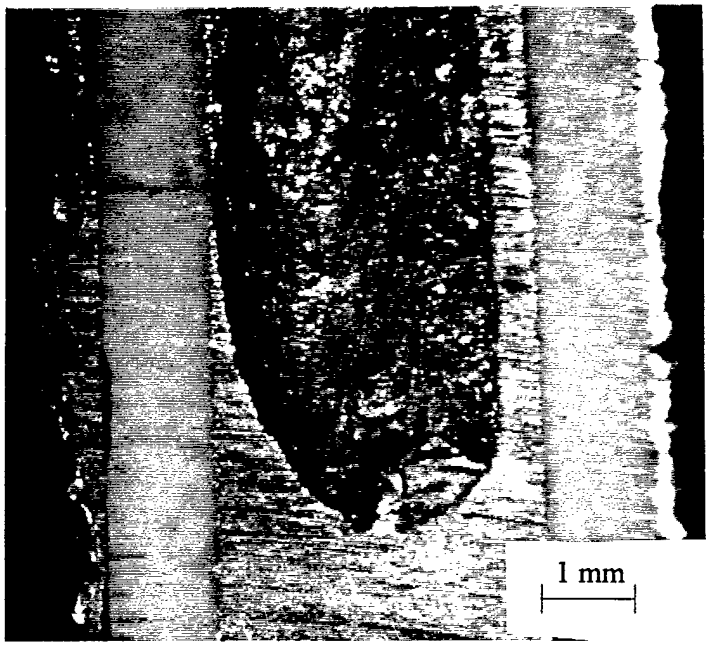

a

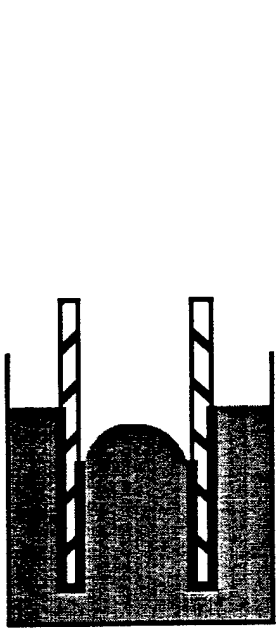

b

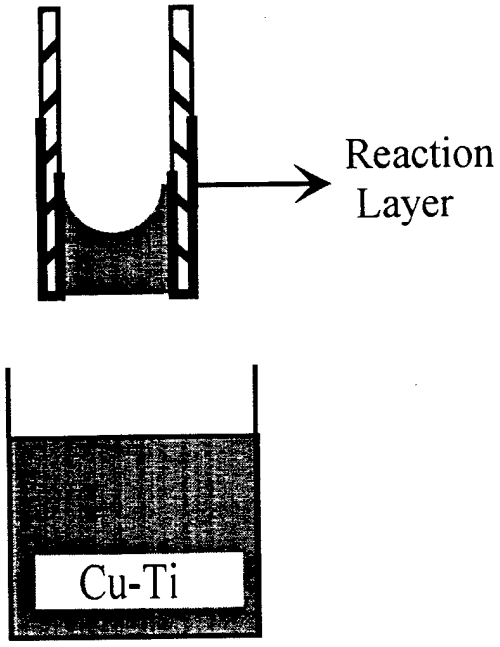

c

Figure 9 The liquid morphology when alumina tube is immersed to greater depth and withdrawn a) cross-sectional macrograph, b) schematic diagram representing the immersed condition and c) schematic diagram representing the withdrawn condition.

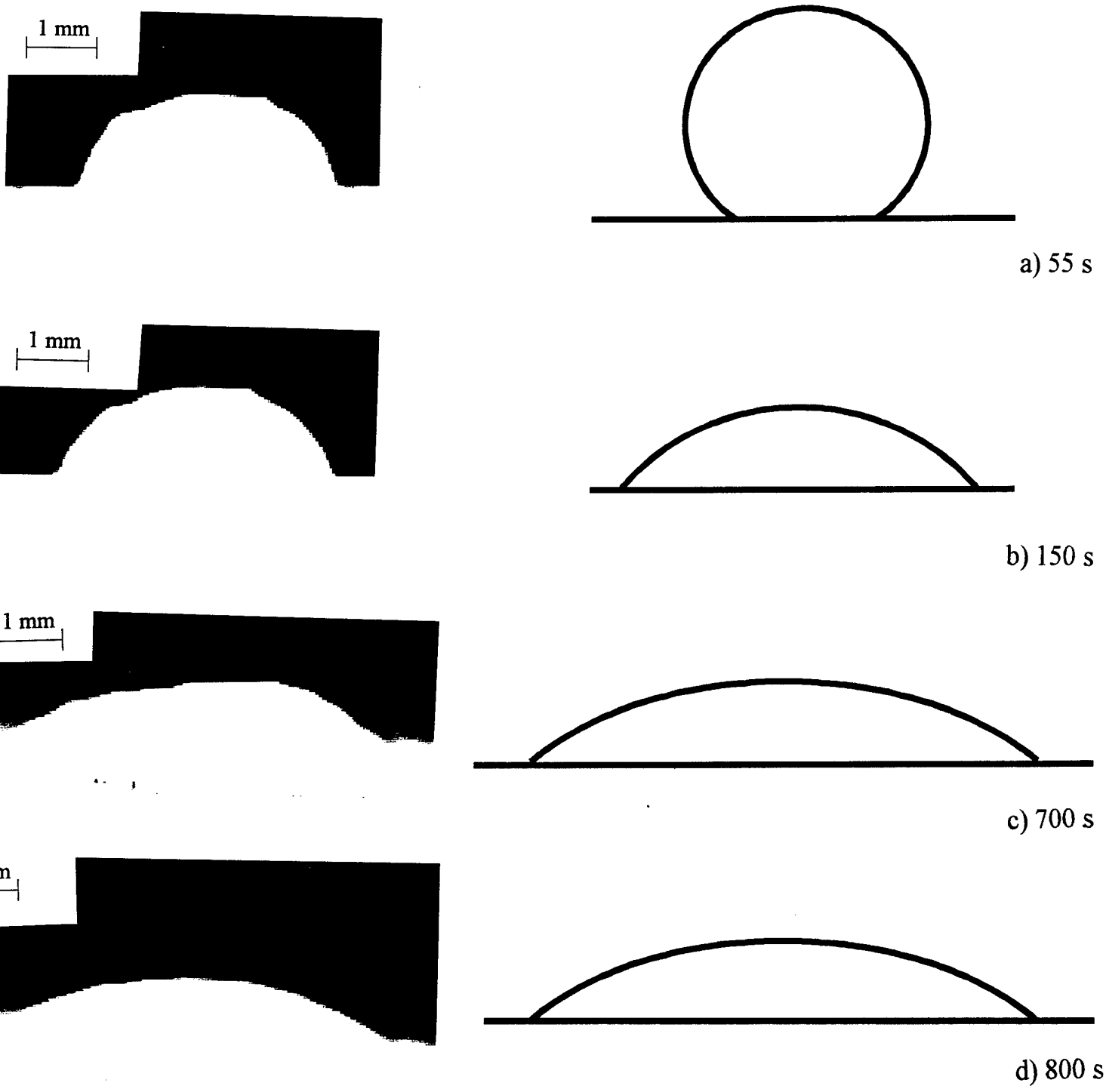

Figure 10 The sessile drop morphologies and the corresponding schematic diagrams for the copper 3-w/o oxygen alloy spreading on alumina substrate at 1300°C.

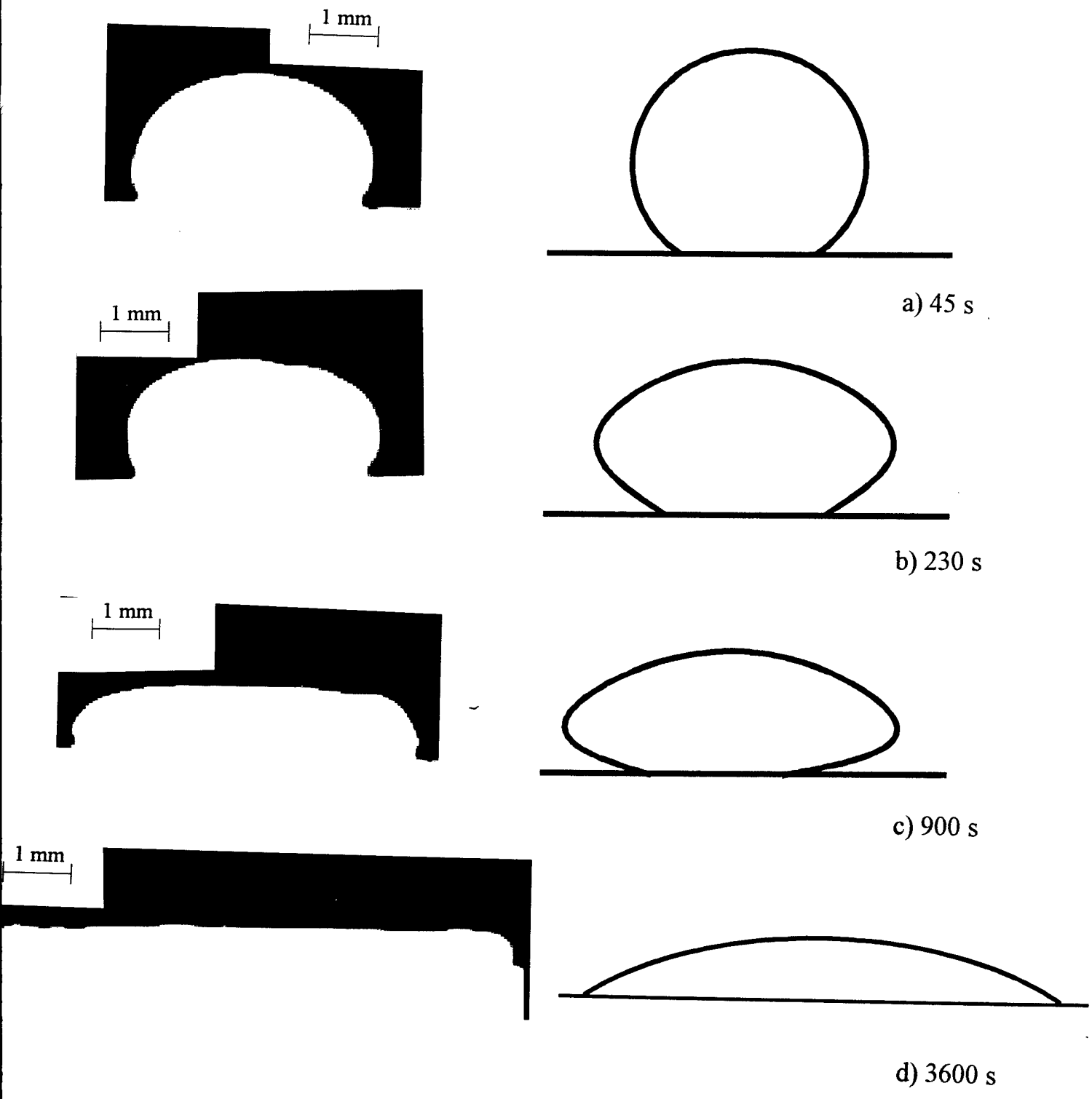

Figure 11 The sessile drop morphologies and the corresponding schematic diagrams for the various stages during the spreading of copper 8.5-w/o titanium alloy on alumina substrate at 1200°C.

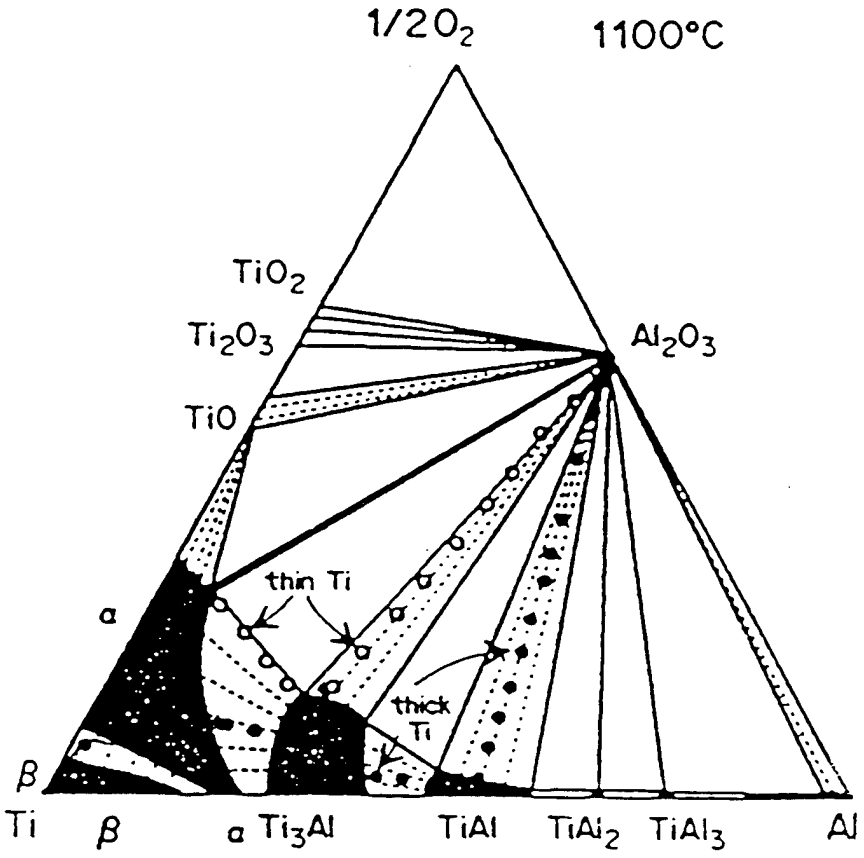

Figure 12 Isothermal section of the Ti-Al-O system at 1100°C proposed by Li *et al.* Taken from X.L. Li, R.H. Hillel, F. Teyssandier, S.K. Choi, and F.J.J. Van Loo, "Reactions and Phase Relations in the Ti-Al-O System", *Acta Met.*, Vol. 40., No. 11, 1992, pp. 3149-3157.

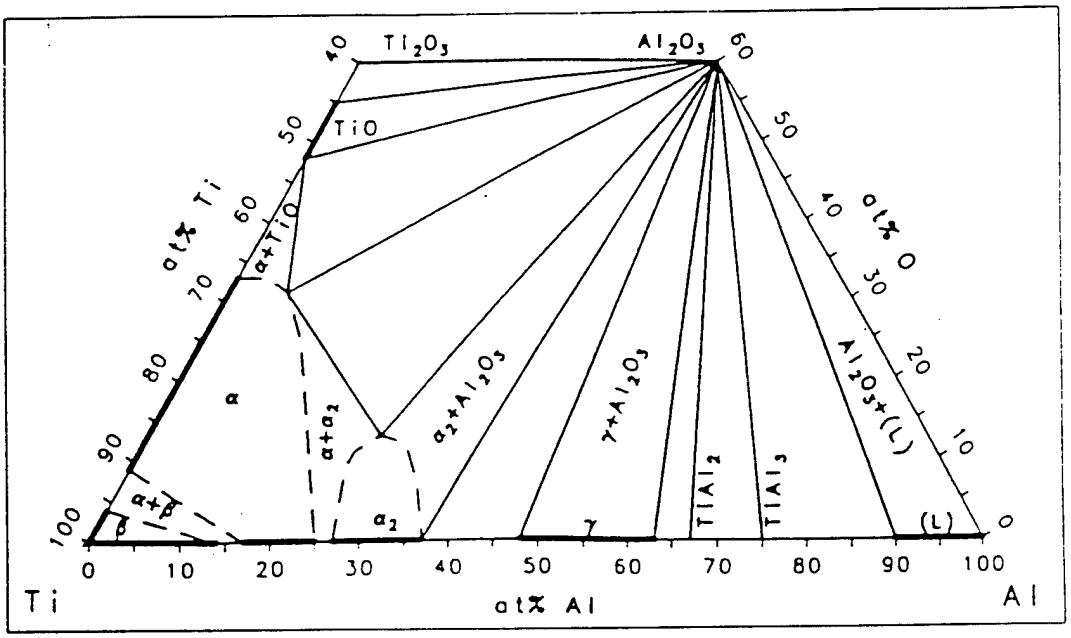

Figure 13 Ti-Al-O constitution diagram at 1100°C, as presented by DeKock *et al.* Taken from J.A. DeKock and Y.A. Chang, "The Stability on Interfaces in High Temperature Metal-Matrix Composites", JOM, March 1993, pp. 21-23.

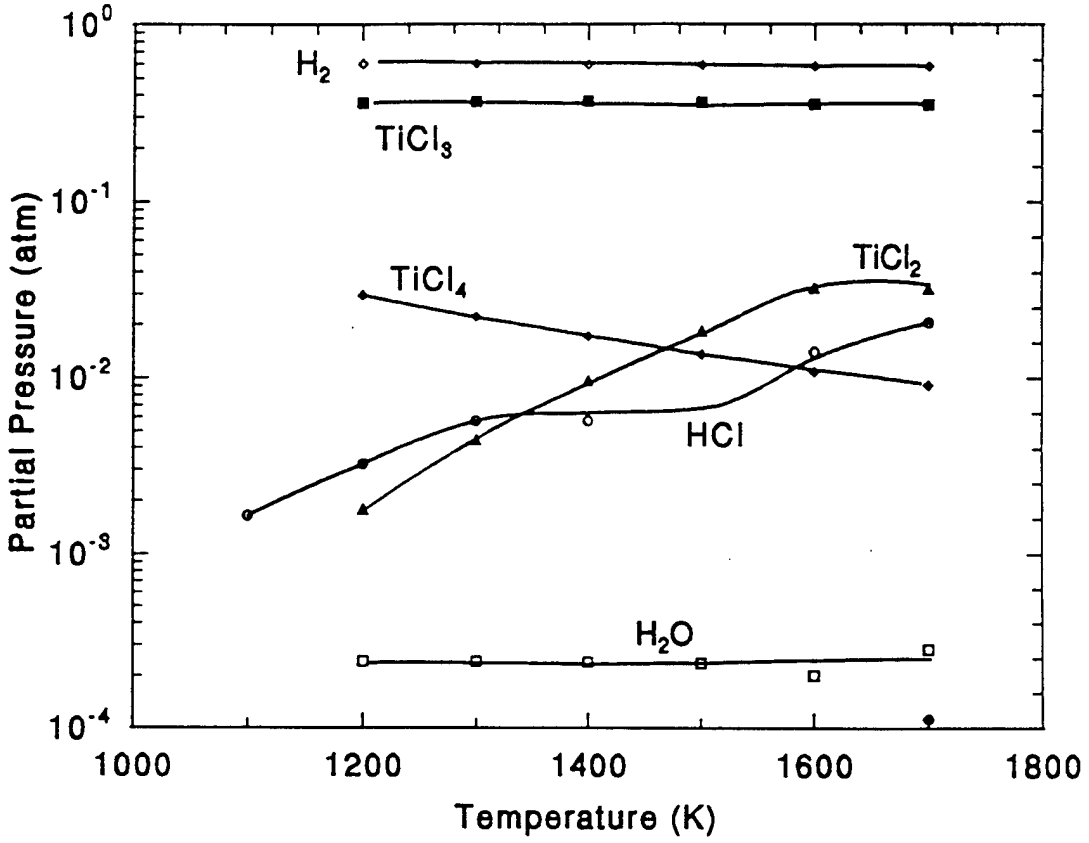

Figure 14 Temperature-partial pressure relations for the dominant gas species for a CVD titanium/hydrogen chloride activated atmosphere.

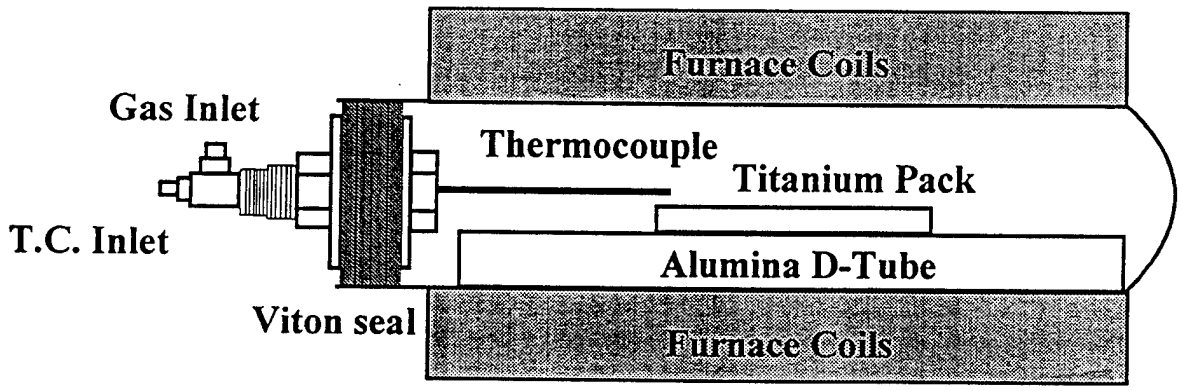

Figure 15 Schematic diagram of the chemical vapor deposition apparatus used for titanium preconditioning of Al_2O_3 substrate material.

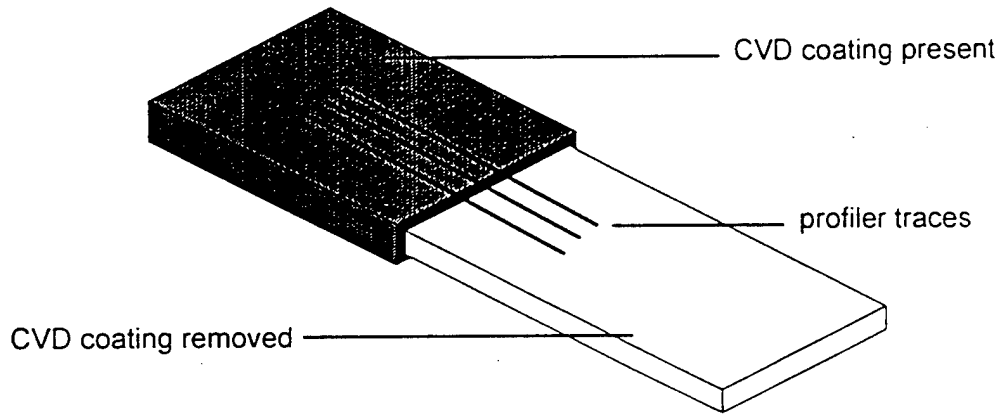

Figure 16 Schematic diagram of a CVD coated Al_2O_3 substrate with part of the coating removed for coating thickness measurement.

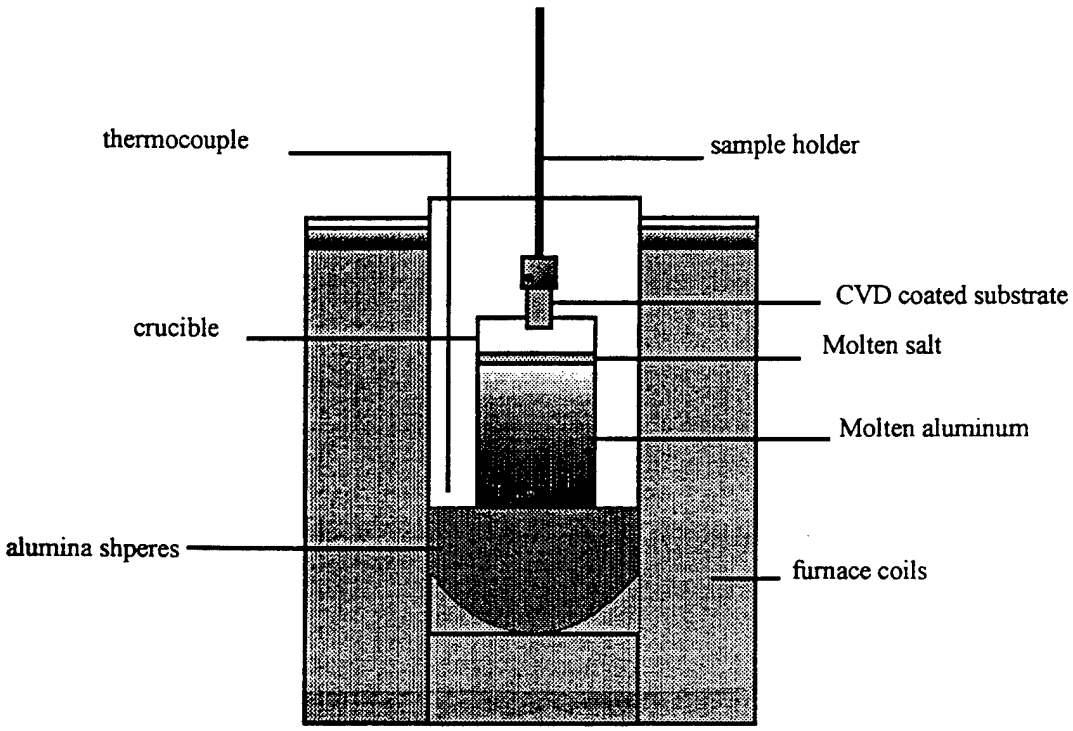

Figure 17 Schematic diagram of the immersion apparatus used for the determination of the wetting behavior of coated and uncoated Al_2O_3 substrates.

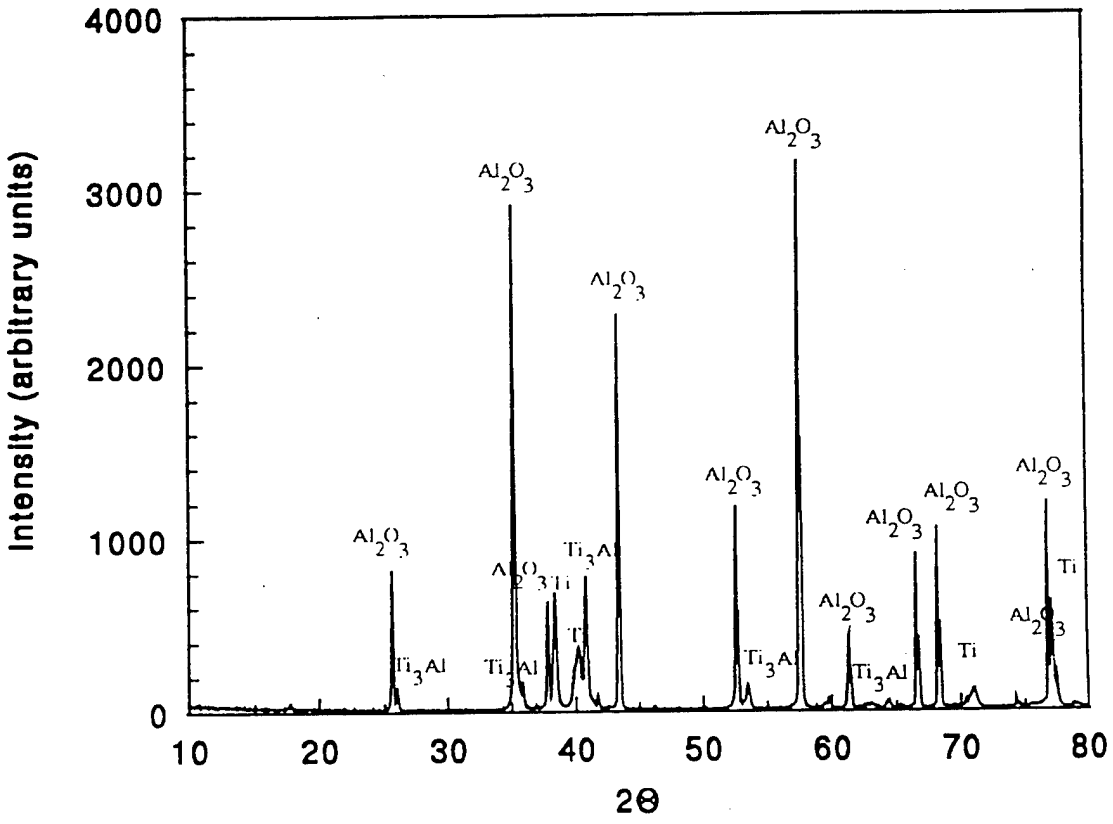

Figure 18 X-Ray diffraction pattern of a CVD coated Al_2O_3 substrate prepared at 729°C with an isothermal coating time of 64.8 kiloseconds.

Figure 19 Backscattered electron image of the interface between a CVD coating and the Al_2O_3 substrate, prepared at 870°C with an isothermal coating time of 64.8 kiloseconds.

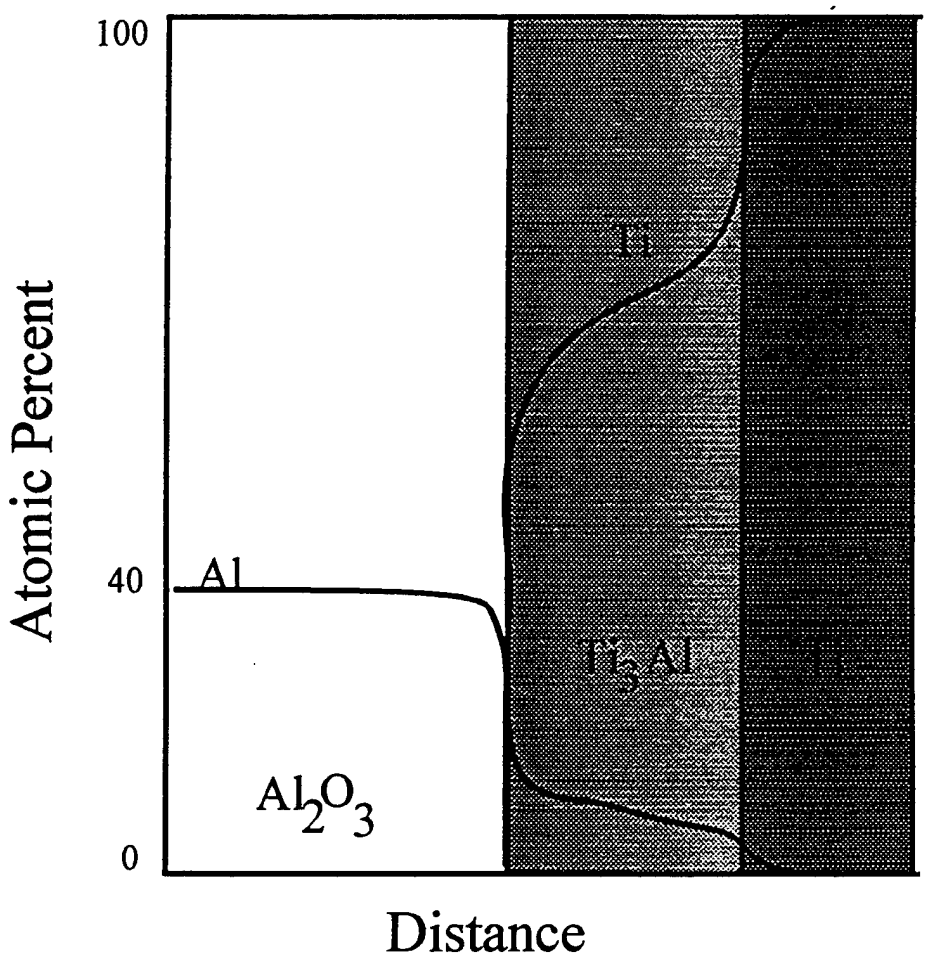

Figure 20 Schematic concentration profile of the coating-substrate interface.

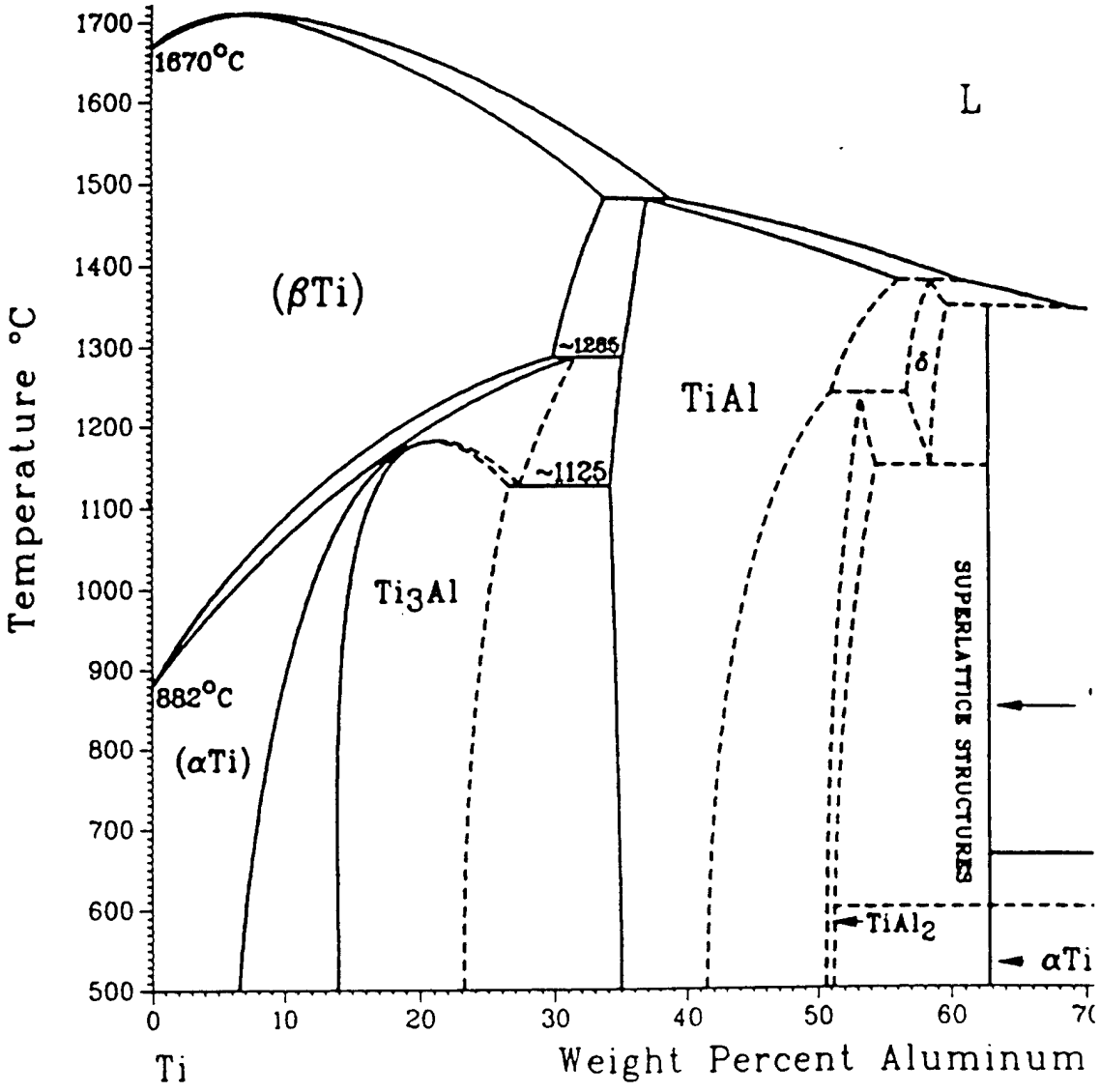

Figure 21 Titanium-rich end of the Aluminum-Titanium phase diagram, taken from *Binary Alloy Phase Diagrams*, J.L. Murray and H.A. Wriedt, 1987.

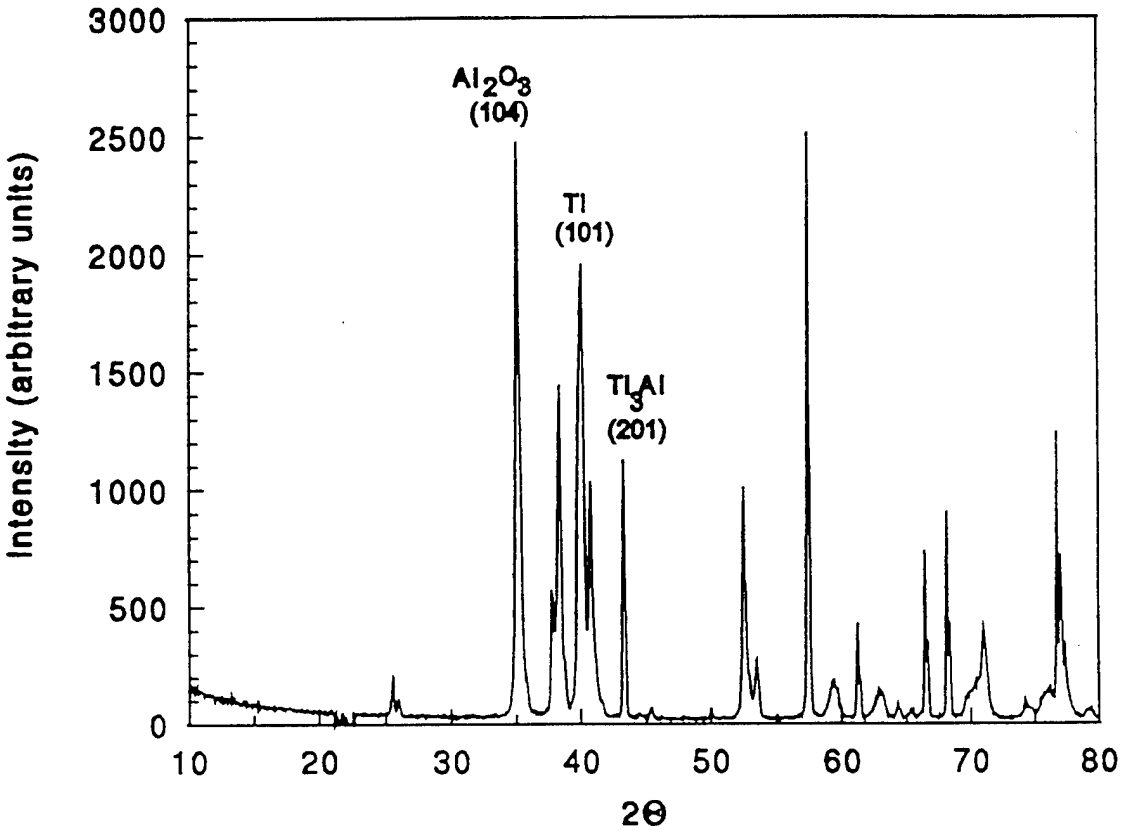

Figure 22 X-Ray diffraction pattern of a CVD coated Al_2O_3 substrate prepared at 870°C with an isothermal coating time of 10.8 kiloseconds.

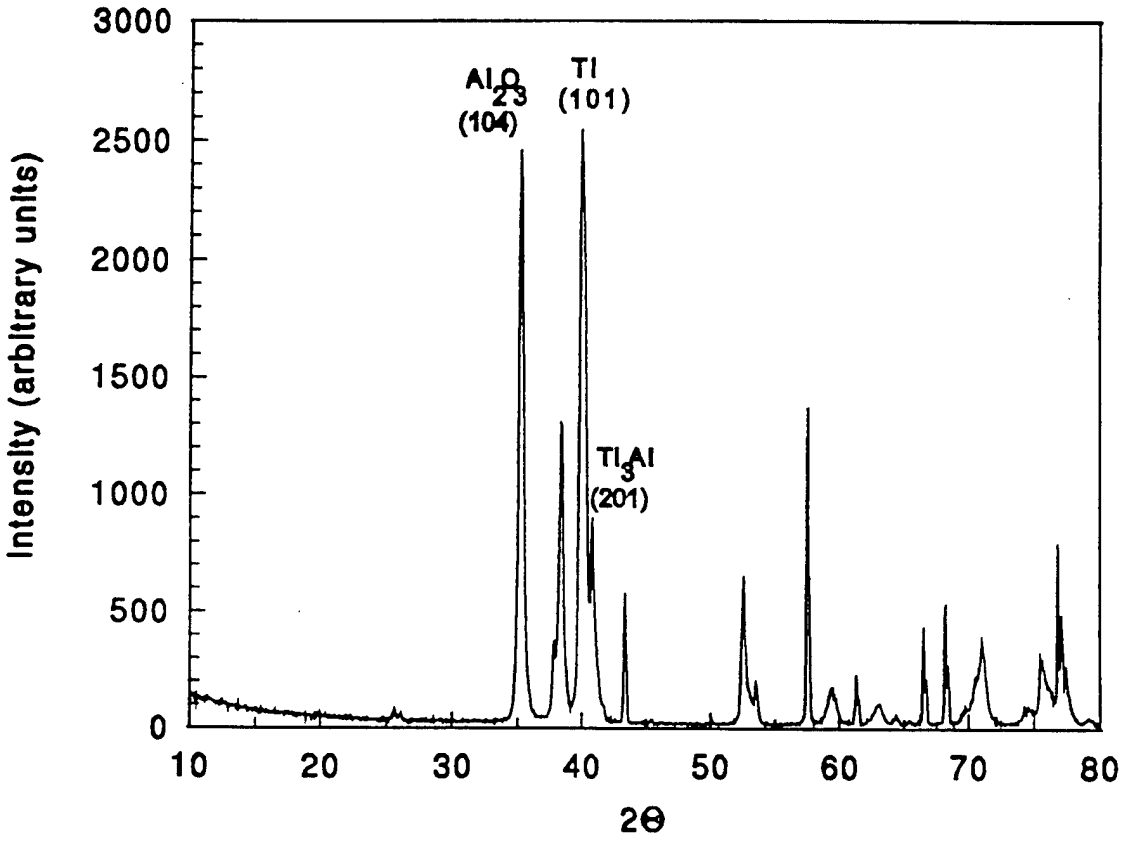

Figure 23 X-Ray diffraction pattern of a CVD coated Al_2O_3 substrate prepared at 870°C with an isothermal coating time of 18.0 kiloseconds.

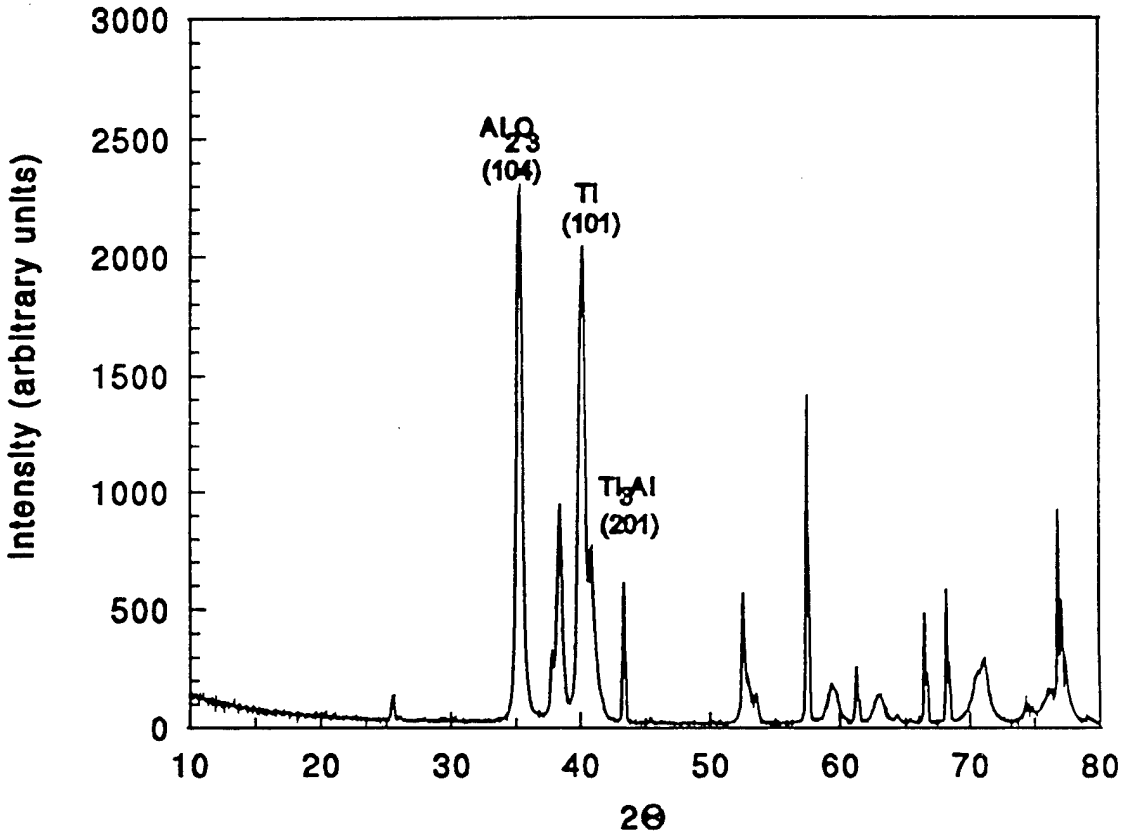

Figure 24 X-Ray diffraction pattern of a CVD coated Al_2O_3 substrate prepared at 870°C with an isothermal coating time of 43.2 kiloseconds

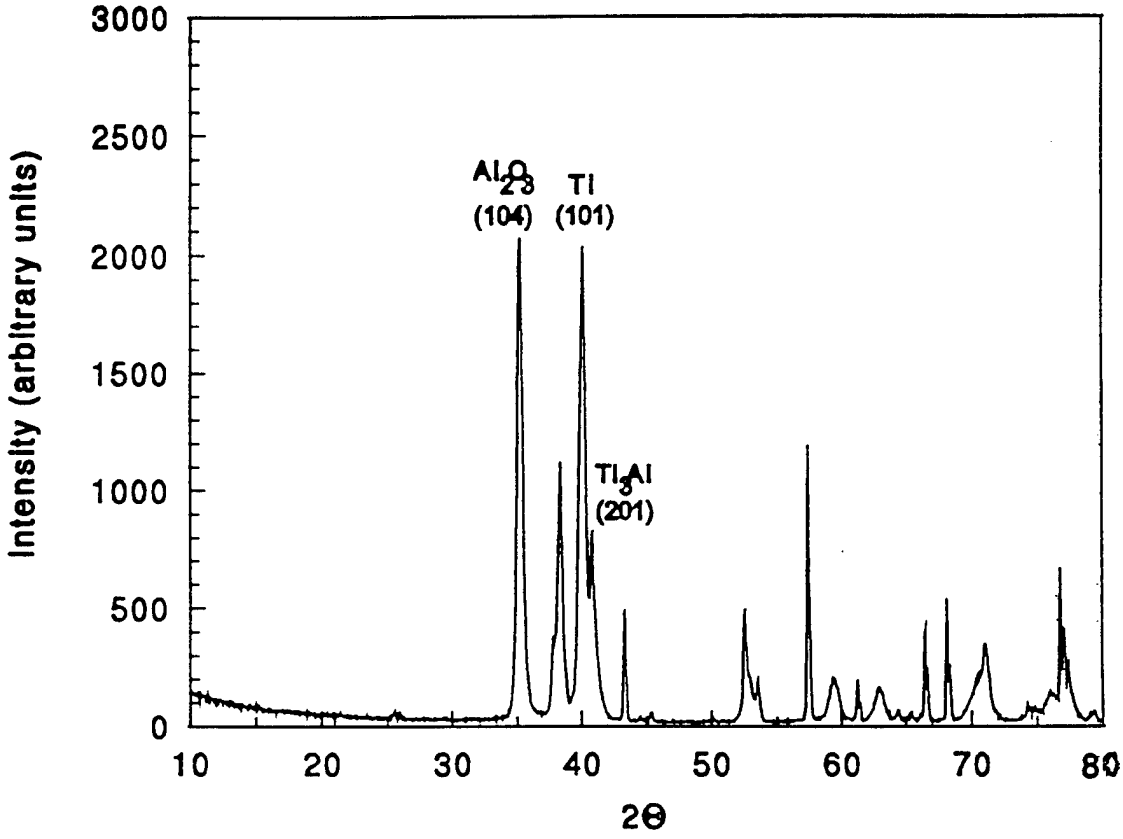

Figure 25 X-Ray diffraction pattern of a CVD coated Al_2O_3 substrate prepared at 870°C with an isothermal coating time of 64.8 kiloseconds.

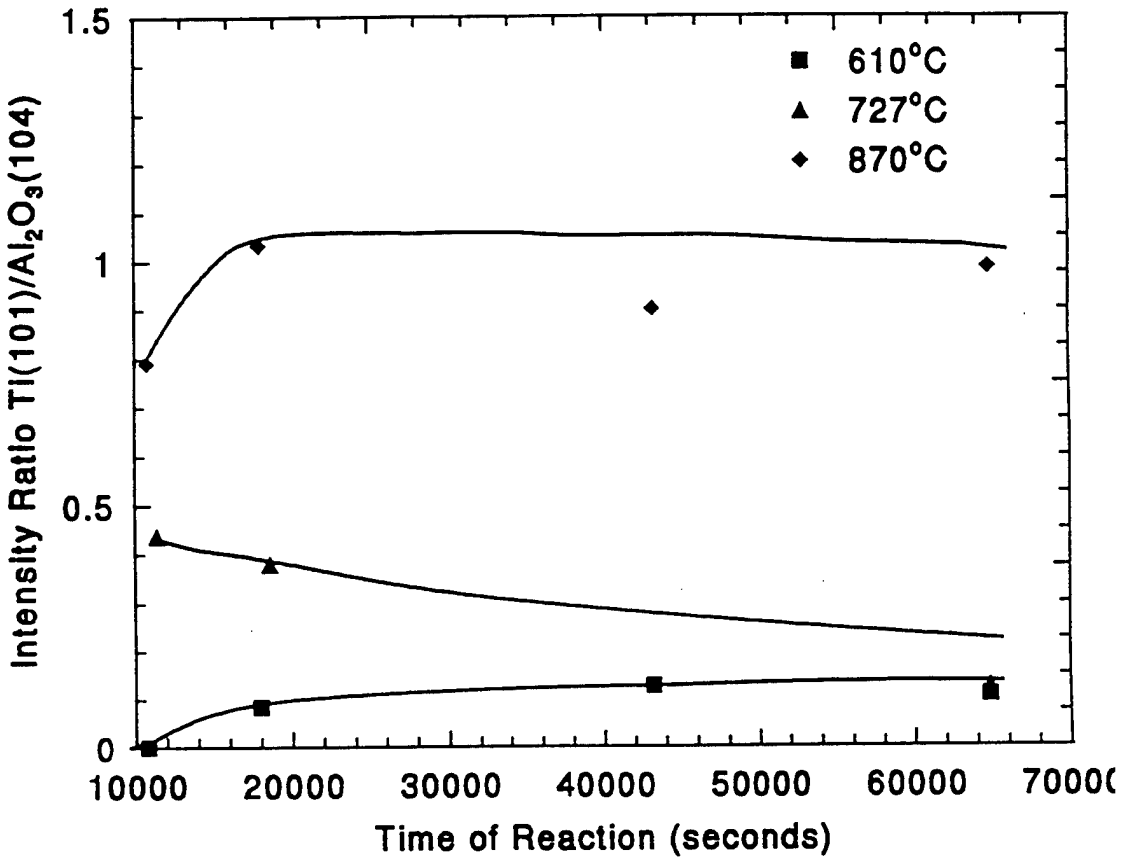

Figure 26 Effects of time and temperature on the normalized intensity (as compared to Al_2O_3 (104)) of the Ti (101) XRD peak for CVD coated Al_2O_3 substrates.

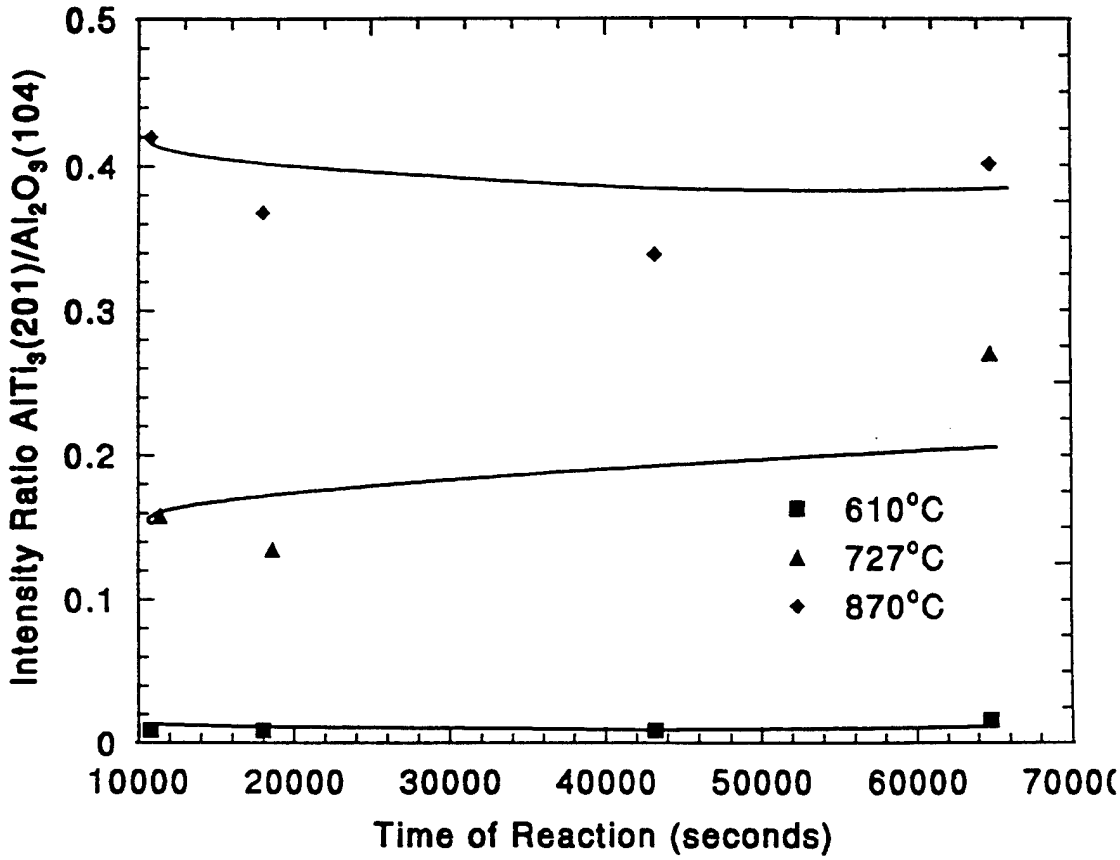

Figure 27 Effects of time and temperature on the normalized intensity (as compared to Al_2O_3 (104)) of the $TiAl_3$ (201) XRD peak for CVD coated Al_2O_3 substrates.

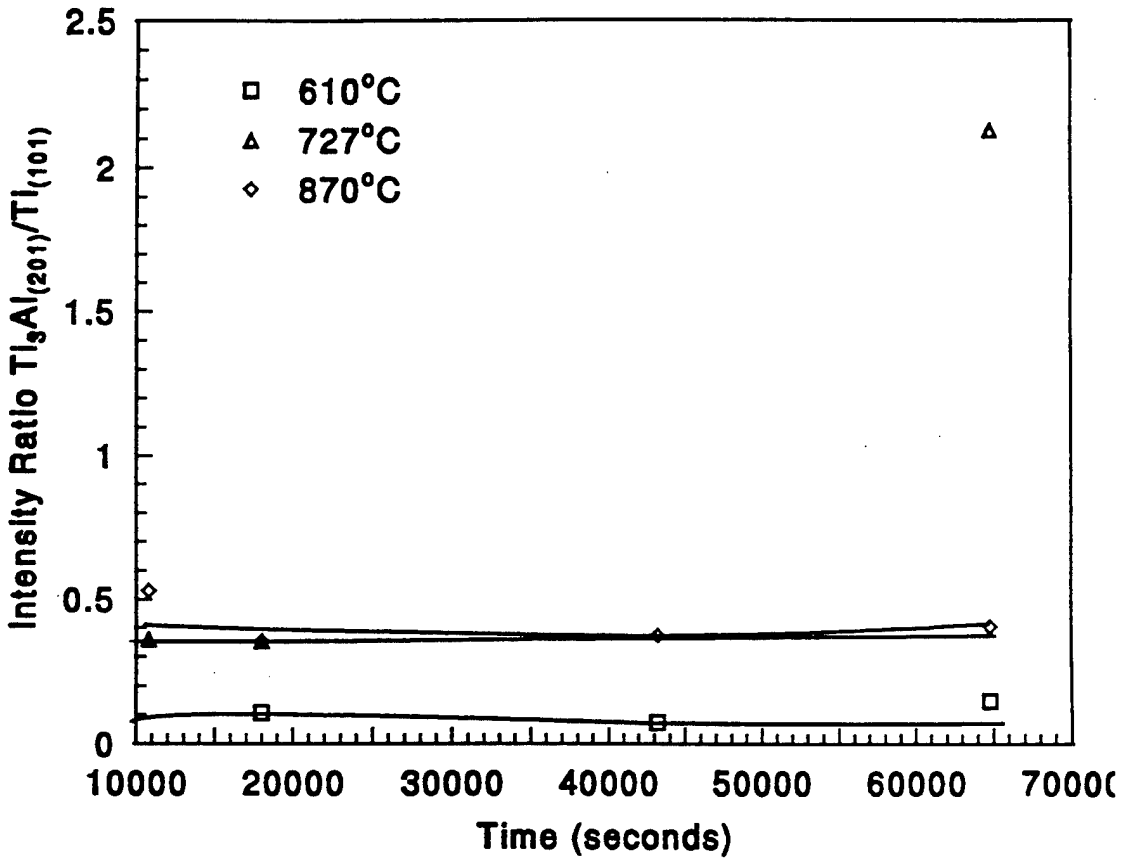

Figure 28 Effects of time and temperature on the intensity of the $TiAl_3$ (201) XRD peak compared to the Ti (101) XRD peak for CVD coated Al_2O_3 substrates.

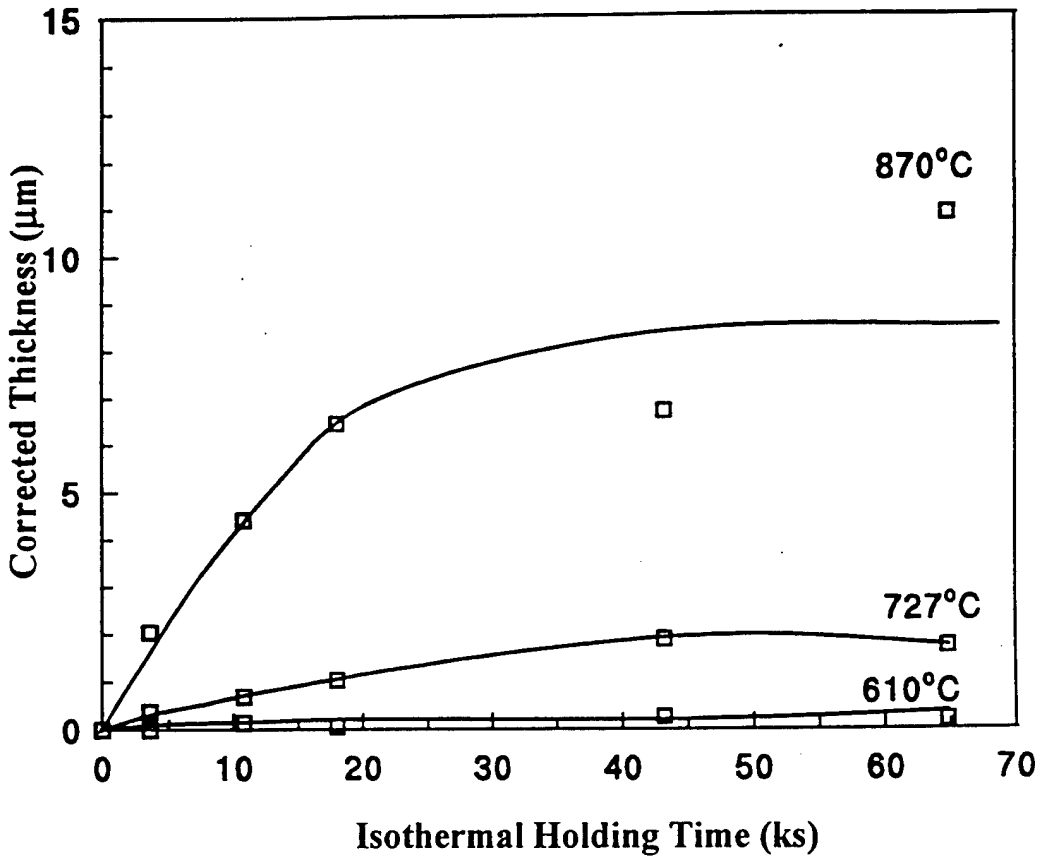

Figure 29 Time dependence of CVD coating thickening for CVD coatings prepared at 610°C, 727°C, and 840°C.

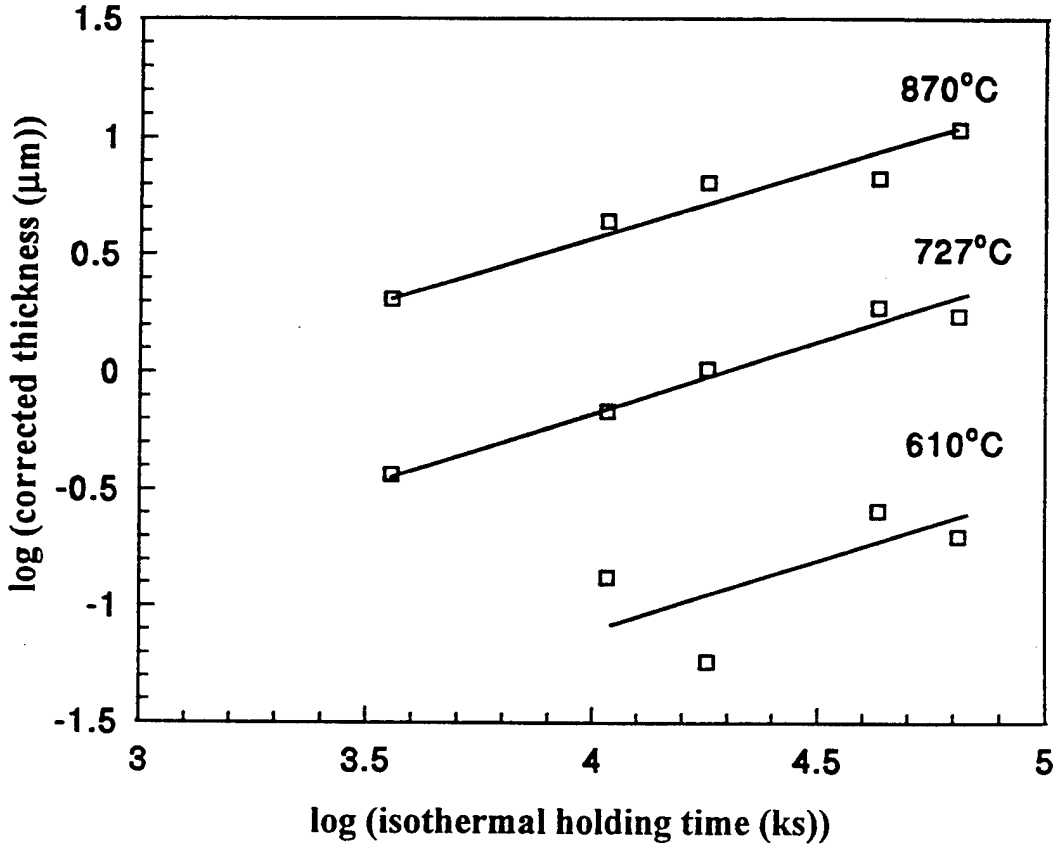

Figure 30 Log time dependence of CVD coating thickening for CVD coatings prepared at 610°C, 727°C, and 870°C.

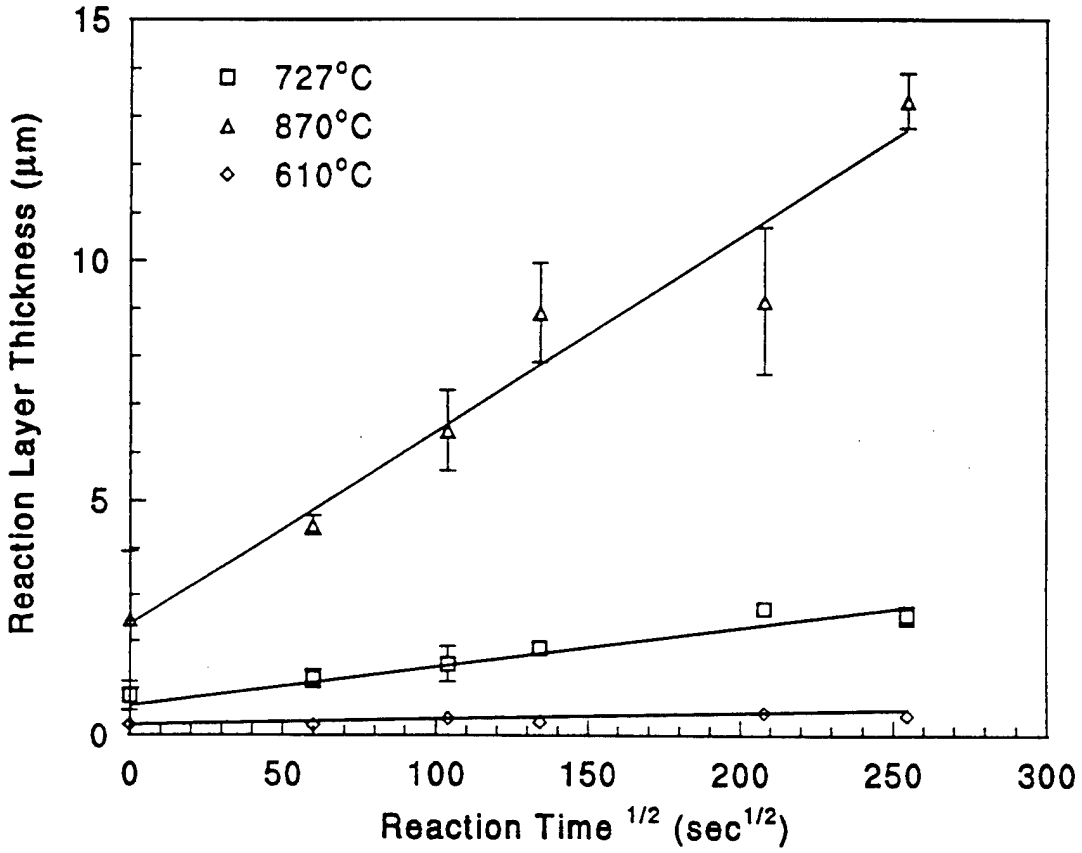

Figure 31 Growth of CVD coatings on Al_2O_3 substrates as a function of time and temperature. Error bars represent 95 percent confidence interval.

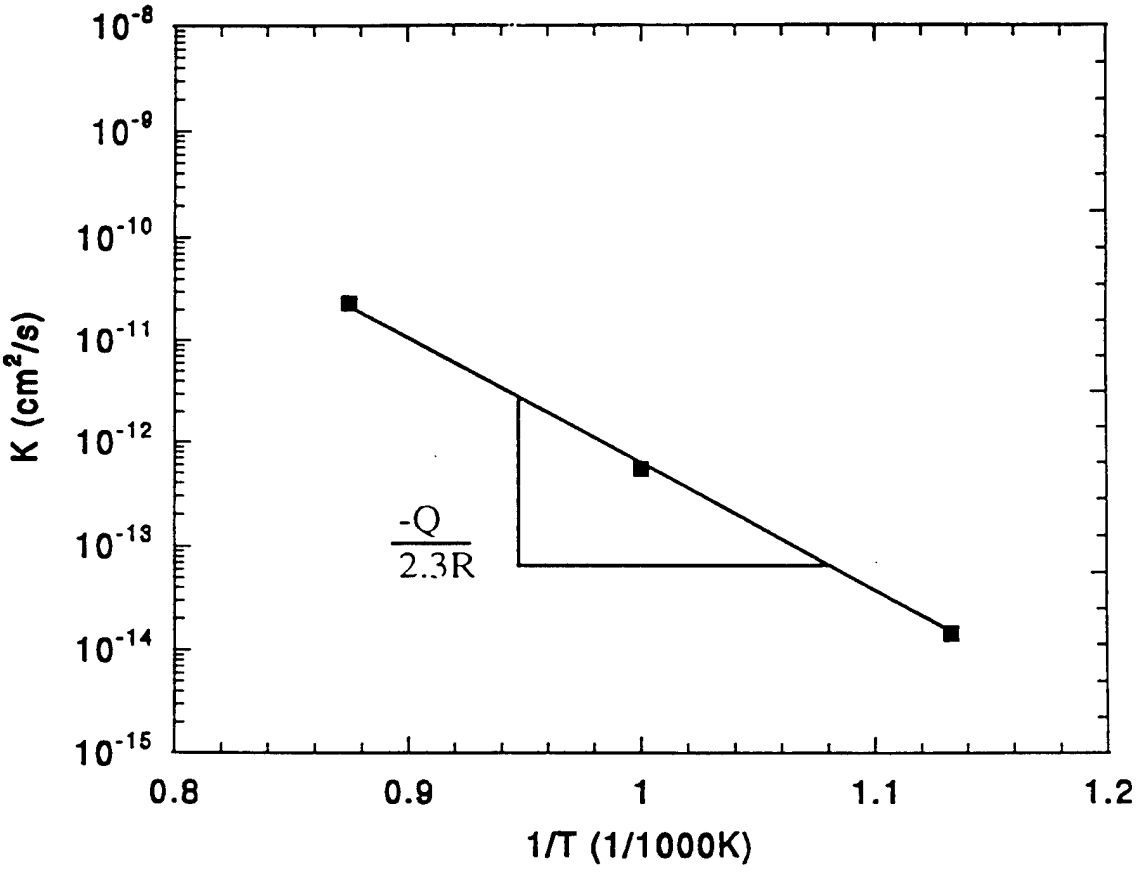

Figure 32 Parabolic rate constants plotted against reciprocal temperature for the growth of CVD coatings on Al_2O_3 substrates. Q = 219 kJmole^{-1}.

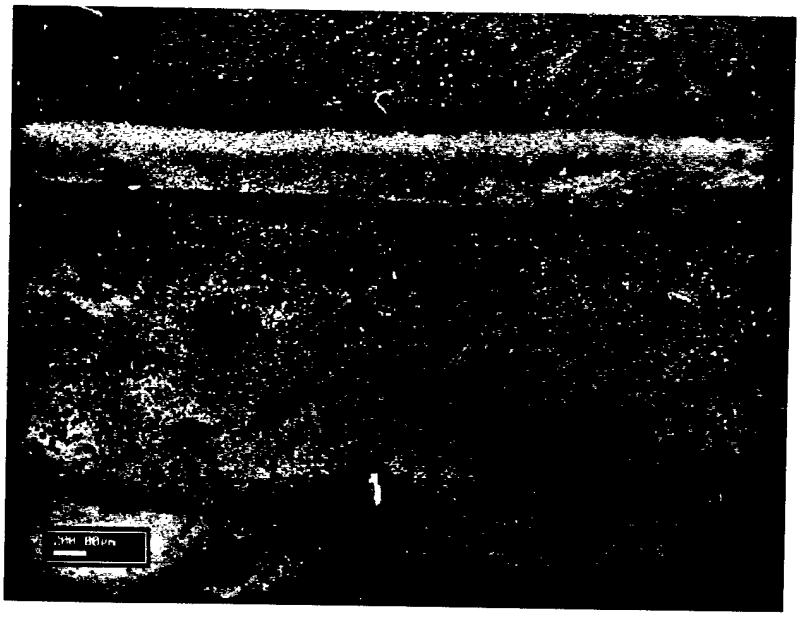

a)

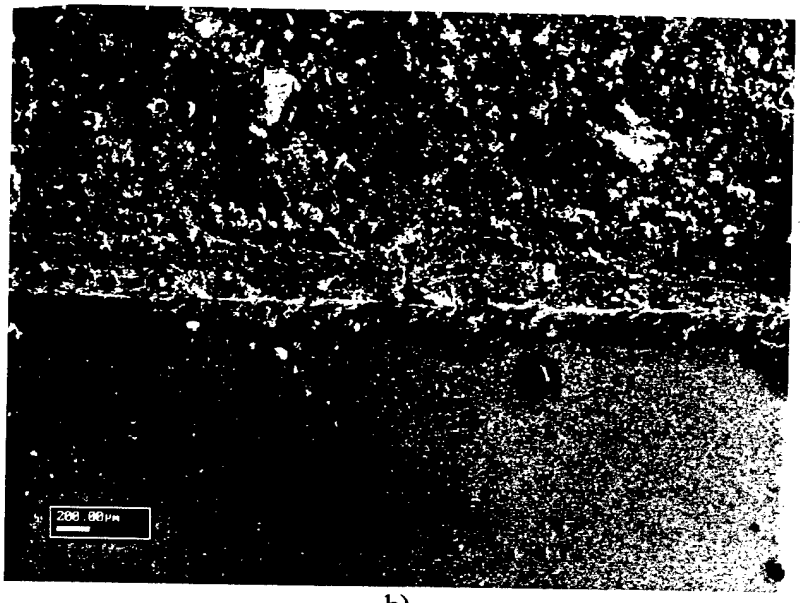

b)

Figure 33 Secondary electron image of the surface of immersion samples in contact with molten aluminum at 1080°C: a) uncoated alumina substrate, holding time of 1.8 kiloseconds (0.5 hour), b) CVD preconditioned alumina substrate, holding time of 10 seconds. CVD coating prepared at 727°C with a holding time of 64.8 kiloseconds (18 hours).

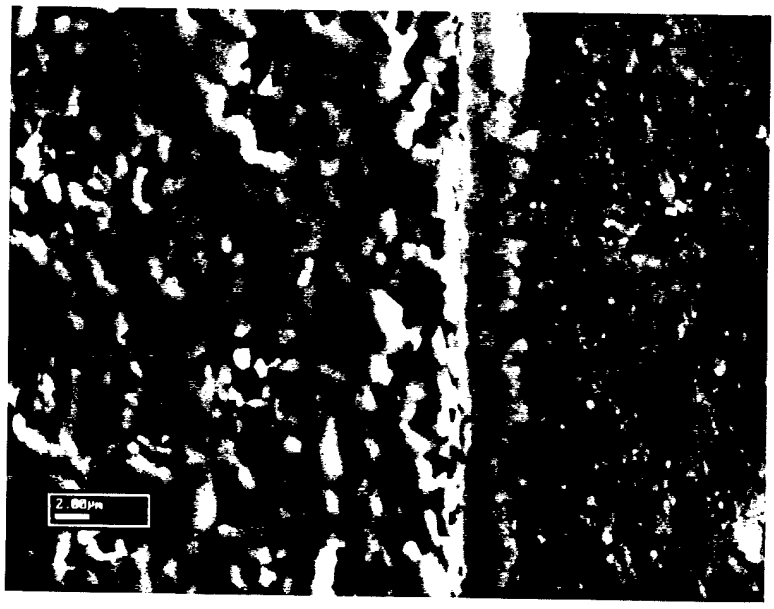

a)

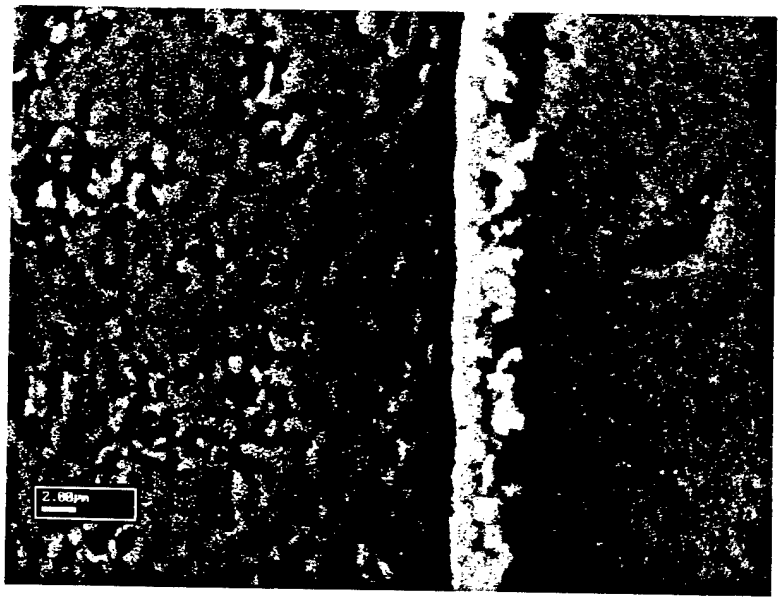

b)

Figure 34 Secondary electron a) and backscattered electron b) images of the interface between a CVD coating on an Al_2O_3 substrate prepared at 727°C with an isothermal holding time of 64.8 kiloseconds (18 hours) in contact with molten aluminum at 950°C, holding time of 10 seconds.

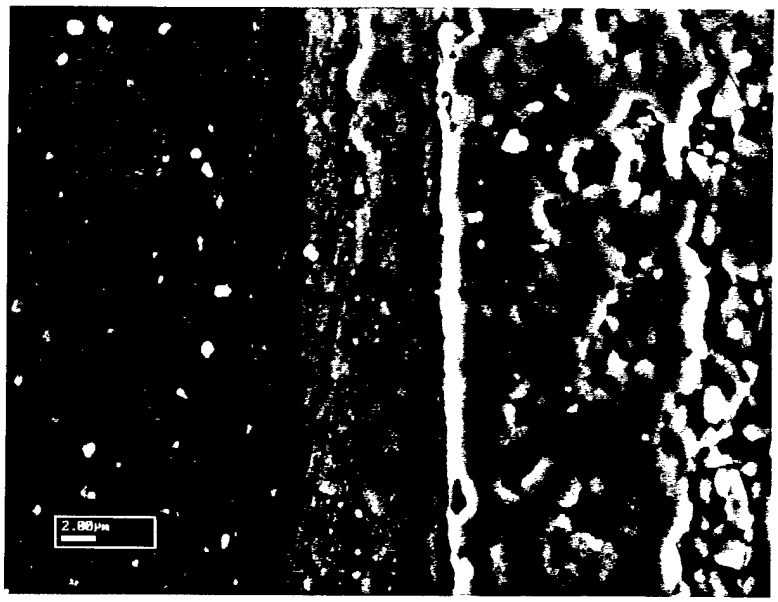

a)

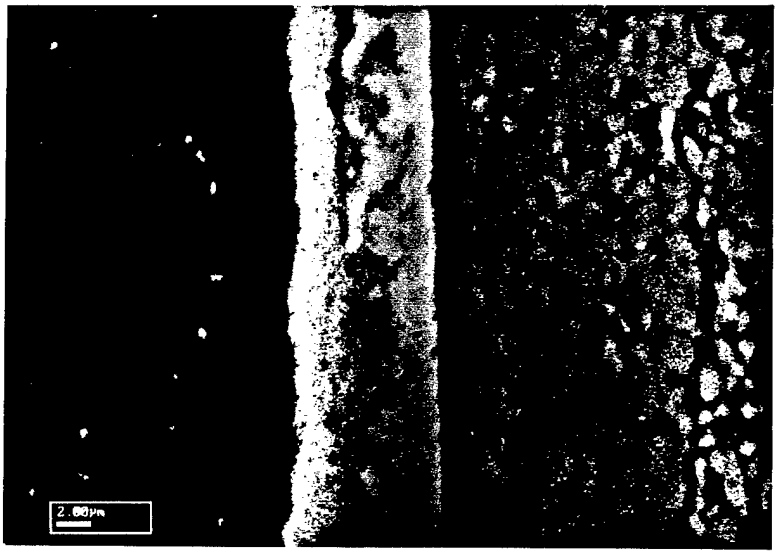

b)

Figure 35 Secondary electron a) and backscattered electron b) images of the interface between a CVD coating on an Al_2O_3 substrate prepared at 727°C with an isothermal holding time of 64.8 kiloseconds (18 hours) in contact with molten aluminum at 950°C, holding time of 30 seconds.

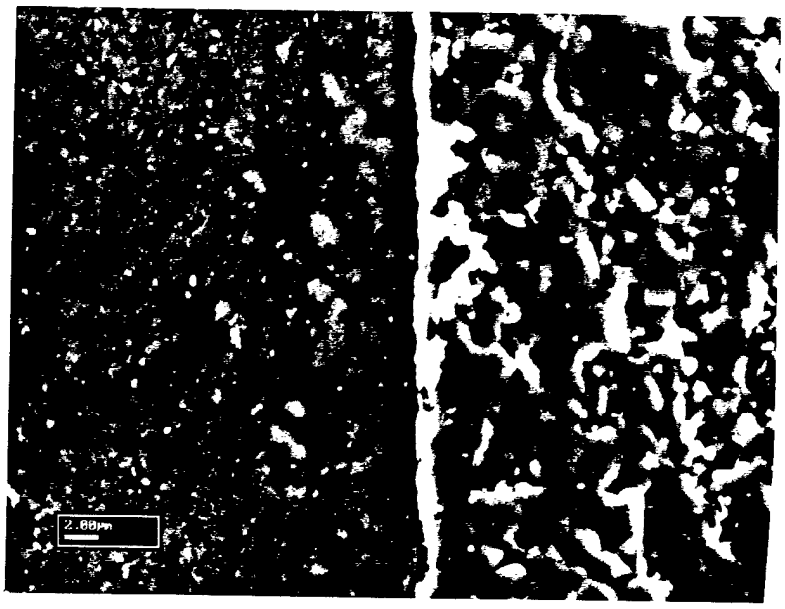

a)

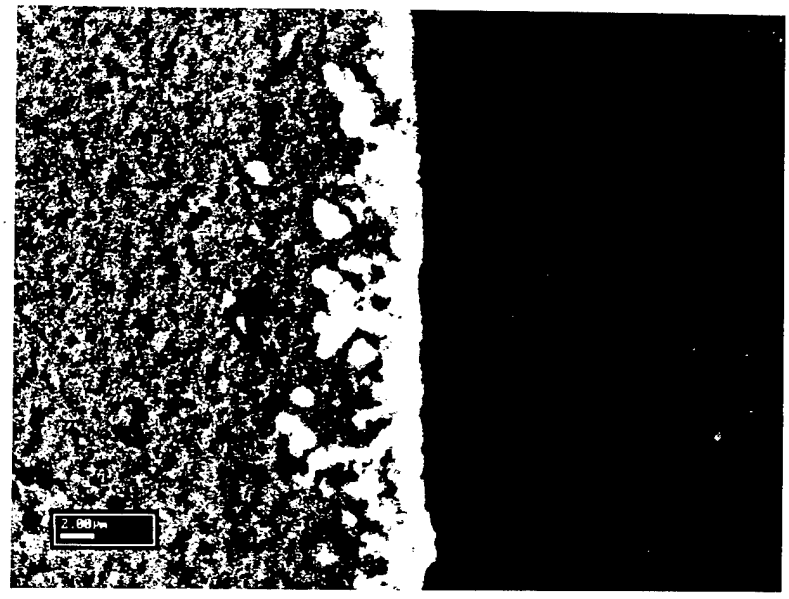

b)

Figure 36 Secondary electron a) and backscattered electron b) images of the interface between a CVD coating on an Al_2O_3 substrate prepared at 727°C with an isothermal holding time of 64.8 kiloseconds (18 hours) in contact with molten aluminum at 950°C, holding time of 60 seconds.

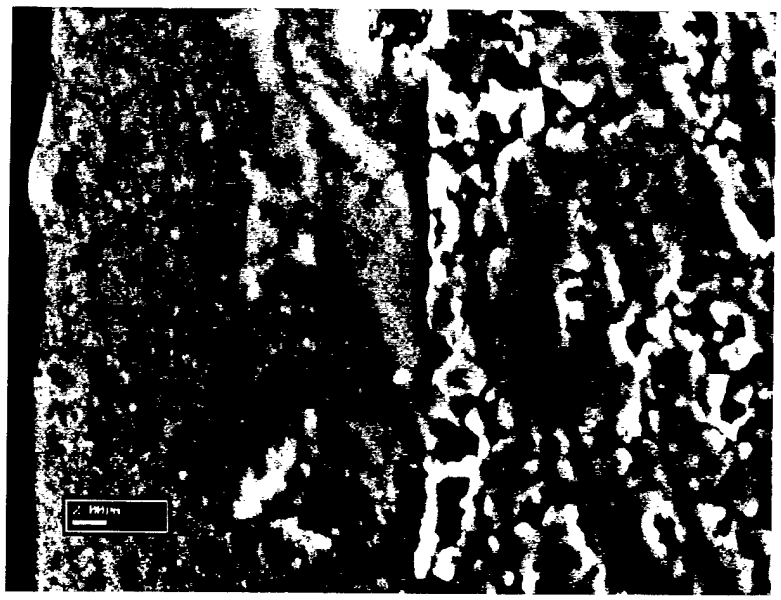

a)

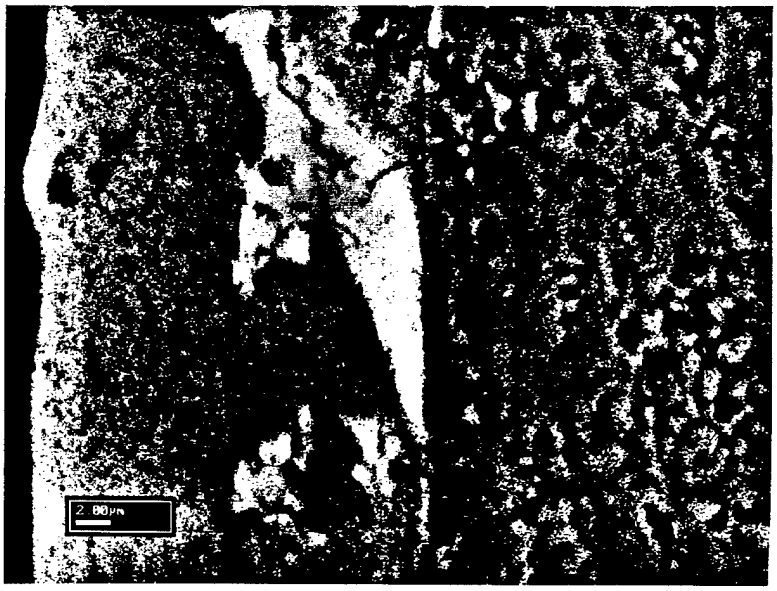

b)

Figure 37 Secondary electron a) and backscattered electron b), images of the interface between a CVD coating on an Al_2O_3 substrate prepared at 727°C with an isothermal holding time of 64.8 kiloseconds (18 hours) in contact with molten aluminum at 1080°C, no holding time.

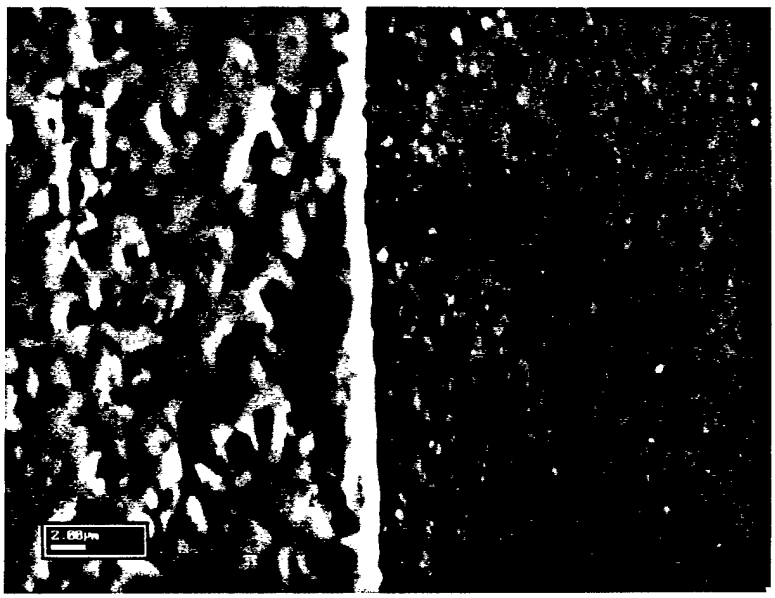

a)

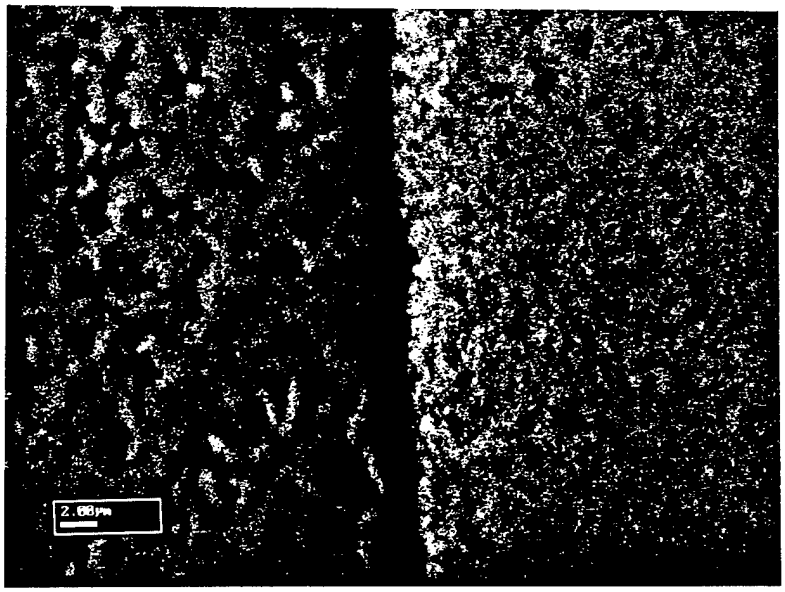

b)

Figure 38 Secondary electron a) and backscattered electron b), images of the interface between a CVD coating on an Al_2O_3 substrate prepared at 727°C with an isothermal holding time of 64.8 kiloseconds (18 hours) in contact with molten aluminum at 1080°C, holding time of 10 seconds.

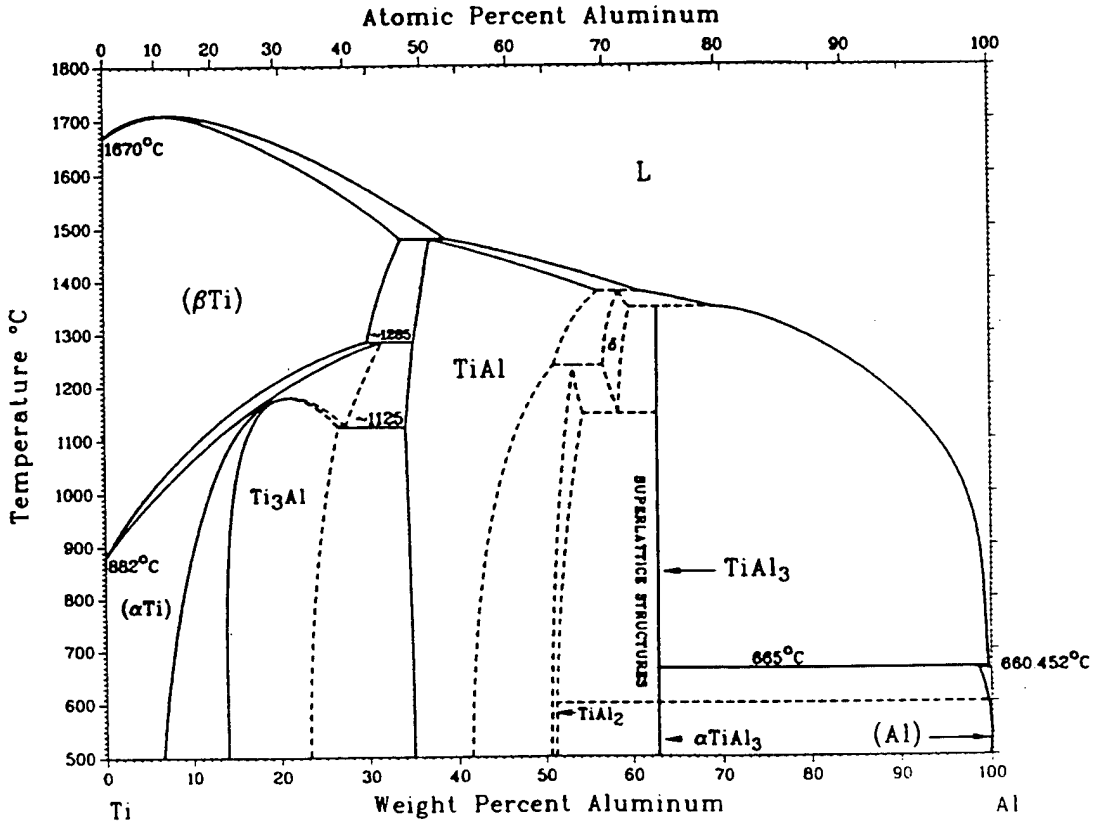

Figure 39 Aluminum-Titanium phase diagram, taken from *Binary Alloy Phase Diagrams*, J.L. Murray and H.A. Wriedt, 1987.

a)

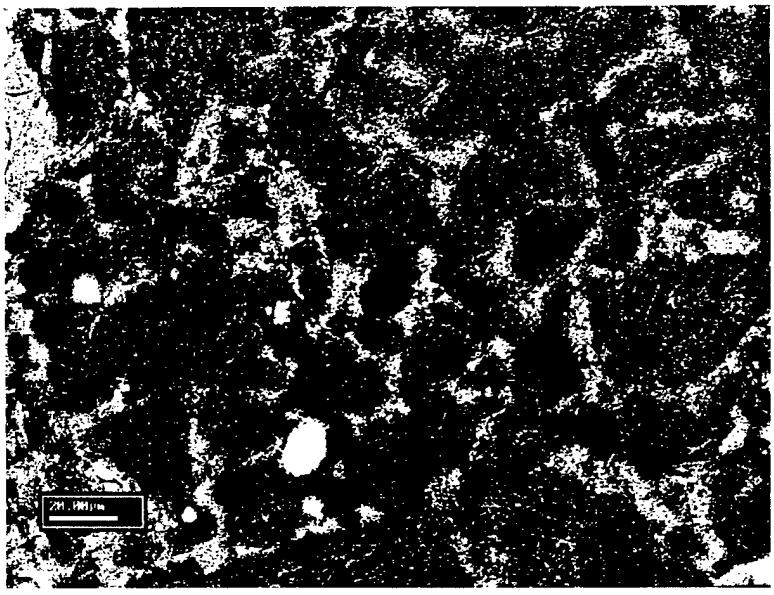

b)

Figure 40 Secondary electron a) and backscattered electron b), images of the cross-section of a 30% porous Al_2O_3 preform prepared with the pack cementation technique at 727°C with an isothermal holding time of 64.8 kiloseconds (18 hours) in contact with molten aluminum at 1100°C with a holding time of 1.8 kiloseconds (0.5 hour).

REFERENCES CITED

1) Naidich, Yu, "Wettability of Solids by Liquid Metals", Prog. in Surf. and Membrane Sci., Vol. l4, p. 353, (l98l)

2) P. Kritsalis, L. Coudurier,and N. Eustathopoulos, J. Mater. Sci., vol. 26, pp. 3400-3408, (1991)

3) P. R. Chidambaram, G. R. Edwards and D. L. Olson, Composite Interfaces, vol. 1, No. 2, p. 127-140, 1993

4) P. R. Chidambaram, G. R. Edwards, and D. L. Olson, Met Trans., vol. 23 B, pp. 215-222, (1992)

5) L. Espie, B. Drevet,and N. Eustathopolous, Metal & Mater Trans A, vol. 25 A, pp. 599-605, (1994)

6) P. Kritsalis, B. Drevet, N. Valignat, and N. Eustathopolous, Scripta Metall. Mater., vol. 30, No. 9, pp. 1127-1132, (1994)

7) Meier. Alan, Chidambaram, P. R. and Edwards, G. R., submitted to J. of Mater. Sci (1994); A. Meier, PhD thesis, T-4665, Colorado School of Mines, (1994)

8) A. Meier, P. R. Chidambaram and G. R. Edwards, J. Mater Sci., in press (1995)

9) M. Baldwin, P. R. Chidambaram and G. R. Edwards, Metal and Mater Trans., Vol. 25 A Nov 1994, pp. 2497 -2506 (1994)

10) M. Ritland, and D. W. Ready, Ceramic Eng. Sc. Proc., Vol. 14, No. 9-10, pp. 896-907 (1993)

11) I. A. Aksay, C. E. Hoge, and J. A. Pask, J. Phys. Chem. vol 78 No. 12 (1974), p. 1178.

12) A. Meier, M. Baldwin, P. R. Chidambaram and G. R. Edwards, Materials Science and Eng., in press (1995)

13) T. B. Massalksi, editor in chief, "Binary Alloy Phase Diagrams", vol. 2, ASM, OH, (1984)

14) M. K. Resser, editor, "Phase Diagram for Ceramists", Am. Ceramic Soc., Columbus, OH, (1964)

15) P. R. Chidambaram, G. R. Edwards, and D. L. Olson, Metal and Mater Trans A, vol. 25 A, pp. 2083-2090, (1994)

16 W. Hunt, "Redefining the limits of Aluminum-Based Materials", JOM, Vol. 45, No. 1, (1993), pp. 18.

17 A. Mortensen, "Interfacial Phenomena in the Solidification Processing of Metal Matrix Composites", Mater. Sci. and Eng., Vol A135, 1991, pp. 1-11.

18 J. Homeny, M.M. Buckley, "Transmission Electron Microscopy Study of an Aluminum Oxide Fiber/Aluminum-Magnesium Alloy Metal Matrix Composite Interface", Mater. Lett., Vol. 10, No. 9, (1991), pp. 421-424.

19 P.R. Chidambaram, Ph.D. Thesis, "Thermodynamic and Kinetic Aspects of Reactive Metals in Contact with Aluminum Oxide", Colorado School of Mines, T-4319, December 1992.

20 G.R. Edwards, Research Proposal #3899, Colorado Schoool of Mines, December (1992).

21 X.L. Li, R. Hillel, F. Teyssandier, S.K. Choi, and F.J.J. Van Loo, "Reactions and Phase relations in the Ti-Al-O System", Acta Metall. Mater, Vol. 40, No. 11, 1992, pp. 3149-3157.

22 R.E. Tressler, T.L. Moore, and R.L. Crane, "Reactivity and Interface Characteristics of Titanium-Alumina composites", J. Mater. Sci., Vol. 8, (1973), pp. 151-161.

23 Per. Kofstad, Nonstoichiometry, Diffusion, and Electrical Conductiviy in Binary Metal Oxides, Wiley Interscience, New York, (1972).

24 P.R. Chidambaram, G.R. Edwards, and D.L. Olson, "Wetting of Ceramic by Molten Metals: Rate Controlling Phenomena", The Metal Sci. of Joining, Edited

by M.J. Cieslak, J.H. Perepezko, S. Kang, and M.E. Glicksman, The Minerals, Metals, and Materials Society, 1992, pp. 67-71.

25 V. Laurent, D. Chatain, C. Chatillon, and N. Eustathopoulos, "Wettability of Monocrystalline Alumina by Aluminum Between its Melting Point and 1273K, Acta Metall., Vol. 36, No. 7, 1988, pp. 1979-1803.

26 J.J. Brennan and J.A. Pask, "Effect of Nature of Surfaces on Wetting of Sapphire by Liquid Aluminum", Jon. of the Amer. Ceram. Soc., Vol. 51, October 1968, pp. 569-573.

27 N. Eustathopoulos, J.C. Joud, P. Desre, and J.M. Hicter, "The Wetting of Carbon by Aluminum and Aluminum Alloys", J. of Mater. Sci., Vol. 9, 1974, pp. 1233-1242.

28 V. de L. Davies, "Influence of Small Additions of Sodium on the Surface Tension of Aluminum and Aluminum-Silicon Alloys", Jon. o f the Institute of Metals, Vol. 92, 1963-64, pp. 208-210.

29 M. Nathan, C.R. Anderson, and J.S. Ahearn, "Interfacial Reactions of Thin Titanium Aluminide Films with Al_2O_3 films and with Sapphire", Mater. Sci. and Engineering, Vol. A162, (1993), pp. 107-113.

30 F. Hatakeyama, K. Suganuma, and T. Okamoto, "Solid-State Bonding of Alumina to Austenitic Stainless Steel", Jon. of Mater. Sci., Vol. 21, (1986), pp. 2455-2461.

31 J.A. DeKock and Y.A. Chang, "The Stability of Interfaces in High-Temperature Metal Matrix Composites", JOM, March 1993, pp. 21-23.

32 F.S. Ohuchi and M. Kohyama, "Electronic Structure and Chemical Reactions at Metal-Alumina and Metal-Aluminum Nitride Interfaces", Jon. Amer. Ceram. Soc., Vol. 74, No. 6, 1991, pp. 1163-1187.

33 B.V. Cockeram, and R.A. Rapp, "The Kinetics of Multilayered Titanium-Silicide Coatings Grown by the Pack Cementation Method", Metall. and Mater. Trans A, Vol. 26A, April 1995, pp. 777-791.

34 L. Vandenbulcke, G. LePrince, and B. Nciri, "Low-pressure Gas-phase Pack Cementation Coating of Complex-shaped Alloy Surfaces", Mater. Sci. and Eng., Vol A121, 1989, pp. 379-386.

35 R. Bianco, M.A. Harper, and R.A. Rapp, "Codepositing Elements by Halide-Activated Pack Cementation", JOM, Vol. 43, No. 11, Nov. 1991, pp. 20-25.

36 S.R. Levine and R.M. Craves, Jon. Electrochem. Soc., 1974, Vol. 121, pp. 1051-1064.

37 R. Bianco and R.A. Rapp: *Jon. Electrochem. Soc.*, 1993, Vol. 140, pp. 1181-1190.

38 A. Mueller, G. Wang, R.A. Rapp, and E.L. Courtright: *Jon. Electrochem. Soc.*, 1992, Vol. 139, pp. 1266-1275.

39 S.C. Kung, and R.A. Rapp: *Oxid. Met.*, 1989, Vol. 32, pp. 89-109.

40 B.K. Gupta, A.K. Sarkhel, and L.L. Seigle: *Thin Solid Films*, 1976, Vol. 39, pp. 313-320.

41 A.J. Hickle and R.W. Heckel: *Metall. Trans. A*, 1975, Vol. 6A, pp. 431-440.

42 C. Wagner: *Z. Phys. Chem. B*, 1993, Vol. B21, pp. 25-41.

43 J.L. Murray and H.A. Wriedt, *Bull. Alloy Phase Diagr.*, Vol. 8, 1987, p. 148.

44 G.Wang, B. Gleeson, and D.L. Douglas, "Phenomenological Treatment of Multilayer Growth ", Oxidation of Metals, Vol. 31, Nos. 5/6, 1989, pp. 415-429.

45 M.A. Dayananda, "Average Effective Interdiffusion Coefficients in Binary and Multicomponent Alloys", Defect and Diffusion Forum, Vol. 95-98, 1993, pp. 521-536